Ortho-Metalation Dynamics and Ligand Fluxionality in the Conversion of Os 3 (CO) 10 (dppm) to HOs 3 (CO) 8 [μ-PhP(C 6 H 4 -μ 2 ,η 1)CH 2 PPh 2]: Experimental and DFT Evidence for...

ARTICLE *in* ORGANOMETALLICS · SEPTEMBER 2010

Impact Factor: 4.13 · DOI: 10.1021/om100475v

4 AUTHORS:

Shih-Huang Huang
University of North Texas
17 PUBLICATIONS **60** CITATIONS
SEE PROFILE

Jason Keith
Colgate University
28 PUBLICATIONS **486** CITATIONS
SEE PROFILE

Michael B Hall
Texas A&M University
360 PUBLICATIONS **10,301** CITATIONS
SEE PROFILE

Michael G Richmond
University of North Texas
261 PUBLICATIONS **2,282** CITATIONS
SEE PROFILE

ORGANOMETALLICS
Article

Organometallics **2010,** *29,* 4041–4057 4041
DOI: 10.1021/om100475v

Ortho-Metalation Dynamics and Ligand Fluxionality in the Conversion of $Os_3(CO)_{10}$(dppm) to $HOs_3(CO)_8[\mu$-PhP(C_6H_4-μ_2,η^1)$CH_2PPh_2]$: Experimental and DFT Evidence for the Participation of Agostic C−H and π-Aryl Intermediates at an Intact Triosmium Cluster

Shih-Huang Huang,[†] Jason M. Keith,[‡] Michael B. Hall,*[,‡] and Michael G. Richmond*[,†]

[†]*Department of Chemistry, University of North Texas, Denton, Texas 76203, and* [‡]*Department of Chemistry, Texas A&M University, College Station, Texas 77843*

Received May 16, 2010

The mechanism for the stepwise conversion of $Os_3(CO)_{10}$(dppm) to $HOs_3(CO)_9[\mu$-PhP-(C_6H_4)$CH_2PPh_2]$ and $HOs_3(CO)_8[\mu$-PhP(C_6H_4-μ_2,η^1)$CH_2PPh_2]$ has been investigated. The octacarbonyl cluster $HOs_3(CO)_8[\mu$-PhP(C_6H_4-μ_2,η^1)$CH_2PPh_2]$ is in rapid equilibrium with the isomer containing a metalated phenyl ring that is bound to a single osmium, $HOs_3(CO)_8[\mu$-PhP(C_6H_4-η^1)-$CH_2PPh_2]$, which in turn captures CO to give $HOs_3(CO)_9[\mu$-PhP(C_6H_4)$CH_2PPh_2]$ in a reaction that is first-order in cluster and CO with a rate constant of $23.9(3) \times 10^{-3}$ M^{-1} s^{-1} at 288 K. The kinetics for the transformation of $HOs_3(CO)_9[\mu$-PhP(C_6H_4)$CH_2PPh_2]$ to $Os_3(CO)_{10}$(dppm) have been studied in toluene over the temperature range 317−340 K and found to be first-order in starting cluster and independent of CO. Important insight into the reductive coupling process was obtained from the carbonylation kinetics employing $DOs_3(CO)_9[\mu$-(Ph-d_2)P(C_6H_3D)CH_2PPh_2-$d_4]$, which was prepared from $Os_3(CO)_{10}$(dppm-d_8) and where all of the ortho sites on the aryl groups contained deuterium. Here, a significant inverse isotope effect ($k_H/k_D = 0.50$) was found, whose origin actually derives from an inverse equilibrium isotope effect, and this supports a preequilibrium phase of the reaction involving a hydride (deuteride) cluster and an intact Os_3 cluster containing a coordinated aryl moiety, prior to the rate-limiting formation of the unsaturated cluster $Os_3(CO)_9$(dppm-P_a,P_e). Experimental proof for the intermediacy of an extremely labile cluster-aryl complex(es) in the proposed preequilibrium step has been demonstrated by photochemical experiments using the isotopically labeled cluster $Os_3(CO)_{10}$(dppm-d_4), where each aryl group contains one ortho hydrogen and deuterium atom. Photolysis of $Os_3(CO)_{10}$(dppm-d_4) in toluene-d_8 gives a 70:30 mixture of the octa- and nonacarbonyl $HOs_3(CO)_{8,9}[\mu$-(Ph-d_1)P(C_6H_3D)CH_2PPh_2-$d_4]$ and $DOs_3(CO)_{8,9}[\mu$-(Ph-d_1)P-(C_6H_4)CH_2PPh_2-$d_4]$, respectively, over the temperature range 243−298 K. These data indicate that the intermediates formed after CO loss are kinetically labile and that the ortho metalation leads to a thermodynamically equilibrated mixture of hydride and deuteride clusters. DFT calculations corroborate the experimental findings and provide crucial details on the nature and lability of those cluster species that do not lend themselves to direct spectroscopic observation.

Introduction

The directed functionalization of relatively unreactive C−H bonds remains a top priority in the field of catalysis.[1] Only recently have the intricacies associated with the intermolecular C−H bond activation of alkane and alkene substrates at mononuclear compounds been unraveled, and the shroud of ambiguity concerning the nature and reactivity of agostic metal-alkane and π metal-arene compounds, the species that typically precede the formal breaking of a C−H bond, has been forever removed.[2] The reaction dynamics for the metal-mediated activation of common and exotic feedstocks have been elucidated through the use of transient spectroscopic and computational methodologies.[3,4] The use of these techniques, especially when utilized in concert, has provided heretofore unprecedented and intimate details into catalytic processes involving the activation of

*Corresponding authors. E-mail: (M.B.H.) mbhall@tamu.edu; (M.G.R.) cobalt@unt.edu.

(1) (a) Bergman, R. G. *Science* **1984**, *223*, 902. (b) Arndtsen, B. A.; Bergman, R. G.; Mobley, T. A.; Peterson, T. H. *Acc. Chem. Res.* **1995**, *28*, 154. (c) Crabtree, R. H. *Chem. Rev.* **1995**, *95*, 987. (d) Shilov, A. E.; Shul'pin, G. B. *Chem. Rev.* **1997**, *97*, 2879. (e) Labinger, J. A.; Bercaw, J. E. *Nature* **2002**, *417*, 507.

(2) For a few representative examples, see: (a) Janowicz, A. H.; Bergman, R. G. *J. Am. Chem. Soc.* **1982**, *104*, 352. (b) Hoyano, J. K.; Graham, W. A. G. *J. Am. Chem. Soc.* **1982**, *104*, 3723. (c) Jones, W. D.; Feher, F. J. *J. Am. Chem. Soc.* **1984**, *106*, 1650. (i) **1986**, *108*, 4814. (d) Buchanan, J. M.; Stryker, J. M.; Bergman, R. G. *J. Am. Chem. Soc.* **1986**, *108*, 1537. (e) Wick, D. D.; Reynolds, K. A.; Jones, W. D. *J. Am. Chem. Soc.* **1999**, *121*, 3974. (f) Northcutt, T. O.; Wick, D. D.; Vetter, A. J.; Jones, W. D. *J. Am. Chem. Soc.* **2001**, *123*, 7257. (g) Churchill, D. G.; Janak, K. E.; Wittenberg, J. S.; Parkin, G. *J. Am. Chem. Soc.* **2003**, *125*, 1403. (h) **1983**, *105*, 3929.

Published on Web 09/01/2010

C−H bonds and the subsequent conversion of the resulting intermediates to commodity chemicals.

The high intrinsic reactivity displayed by those unsaturated species able to activate hydrocarbon substrates can also lead to the deleterious activation of an auxiliary ligand(s) in the coordination sphere of the metal. In the case of metal-bound phosphine ligands, C−P and C−H bond cleavage manifolds are common, and these reactions are undesirable, as they are believed to retard the catalytic activity of certain reactions.[5] The activation of alkyl and aryl C−H bonds in coordinated phosphine ligands gives rise to cyclometalation and ortho-metalation products, respectively. Interestingly, the exact mechanism associated with the above phosphine activation processes is far from clear,[6] and while one would assume that these ligand-based C−H activations would follow reactivity paths analogous to those systems whose intermolecular activation of hydrocarbons is now well understood, the situation remains, for the most part, largely unaddressed. In an early landmark study, Jones investigated the selectivity of different unsaturated Cp*Rh(I) species for their intramolecular metalation reactivity (ortho and cyclo) at the ancillary phosphine ligands versus intermolecular activation of benzene.[7] Here, the kinetic and thermodynamic aspects related to intra- and intermolecular C−H bond activation were dissected, and the data unequivocally revealed a pronounced thermodynamic preference for the intramolecular activation of the ancillary P-ligand and a kinetic preference for intermolecular C−H bond activation of the benzene solvent.

The ligand activation described above is not limited to mononuclear entities and, in fact, has been observed in numerous polynuclear metal clusters. Unlike their mononuclear counterparts, polynuclear entities display an added dimension of complexity, as contiguous metal centers often promote the multisite activation of a cluster-bound ligand, leading to reactivity patterns that have no parallel in mononuclear coordination chemistry.[8] For example, thermolysis of the diphosphine-bridged cluster $Os_3(CO)_{10}$(dppm) leads to the formation of the ortho-metalated cluster $HOs_3(CO)_8$-[μ-PhP(C_6H_4-μ_2,η^1)CH_2PPh_2], as depicted in eq 1.[9] Two points are noteworthy as it pertains to this octacarbonyl cluster: (1) C−H bond formation is readily reversible under CO, and (2) it remains an active platform for the construction of a plethora of triosmium clusters, whose synthesis and isolation would otherwise be hampered through traditional thermal activation of $Os_3(CO)_{10}$(dppm).[10,11]

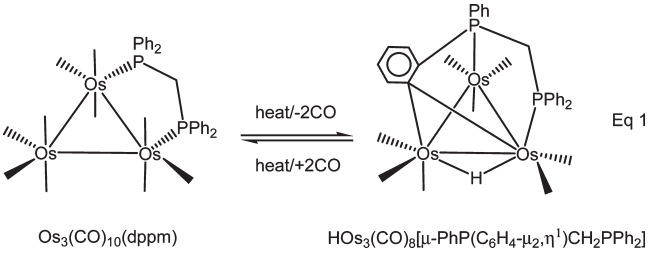

Eq 1

Our groups maintain an interest in the mechanistic and computational study of metal cluster compounds, especially those systems that exhibit an enhanced activation of small molecules and bidentate ligands.[12,13] Recently one of us (M. G.R.) has published a study concerning the ortho metalation of the chelating diphosphine in the cluster $Os_3(CO)_{10}$(bpcd) [where bpcd = 4,5-bis(diphenylphosphino)-4-cyclopentene-1,3-dione].[14] Thermolysis or photolysis of $Os_3(CO)_{10}$(bpcd) leads to CO loss and ortho metalation of one of the aryl substituents to give the hydride cluster $HOs_3(CO)_9$[μ-PhP-(C_6H_4)C=C(PPh_2)C(O)CH_2C(O)]. Treatment of the resulting hydride with CO quantitatively regenerates $Os_3(CO)_{10}$(bpcd)

(3) (a) Whittlesey, M. K.; Mawby, R. J.; Osman, R.; Perutz, R. N.; Field, L. D.; Wilkinson, M. P.; George, M. W. *J. Am. Chem. Soc.* **1993**, *115*, 8627. (b) Schultz, R. H.; Bengali, A. A.; Tauber, M. J.; Weiller, B. H.; Wasserman, E. P.; Kyle, K. R.; Moore, C. B.; Bergman, R. G. *J. Am. Chem. Soc.* **1994**, *116*, 7369. (c) Bengali, A. A.; Schultz, R. H.; Moore, C. B.; Bergman, R. G. *J. Am. Chem. Soc.* **1994**, *116*, 9585. (d) Bromberg, S. E.; Lian, T.; Bergman, R. G.; Harris, C. B. *J. Am. Chem. Soc.* **1996**, *118*, 2069. (e) Blake, A. J.; George, M. W.; Hall, M. B.; McMaster, J.; Portius, P.; Sun, X. Z.; Towrie, M.; Webster, C. E.; Wilson, C.; Zarić, S. D. *Organometallics* **2008**, *27*, 189. (f) Calladine, J. A.; Vuong, K. Q.; Sun, X. Z.; George, M. W. *Pure Appl. Chem.* **2009**, *81*, 1667.

(4) (a) Niu, S.; Zarić, S.; Bayse, C. A.; Strout, D. L.; Hall, M. B. *Organometallics* **1998**, *17*, 5139. (b) Bergman, R. G.; Cundari, T. R.; Gillespie, A. M.; Gunnoe, T. B.; Harman, W. D.; Klinckman, T. R.; Temple, M. D.; White, D. P. *Organometallics* **2003**, *22*, 2331. (c) Hartwig, J. F.; Cook, K. S.; Hapke, M.; Incarvito, C. D.; Fan, Y.; Webster, C. E.; Hall, M. B. *J. Am. Chem. Soc.* **2005**, *127*, 2538. (d) Evans, M. E.; Li, T.; Vetter, A. J.; Rieth, R. D.; Jones, W. D. *J. Org. Chem.* **2009**, *74*, 6907. (e) Zhu, H.; Ziegler, T. *Organometallics* **2009**, *28*, 2773. (f) Yang, Z.; Hall, M. B. *J. Phys. Chem. A* **2009**, *113*, 2152. (g) Flener-Lovitt, C.; Woon, D. E.; Dunning, T. H., Jr.; Girolami, G. S. *J. Phys. Chem. A* **2010**, *114*, 1843. (h) Balcells, D.; Clot, E.; Eisenstein, O. *Chem. Rev.* **2010**, *110*, 749.

(5) (a) Lavigne, G.; de Bonneval, B. In *Catalysis by Di- and Polynuclear Metal Cluster Complexes*; Adams, R. D.; Cotton, F. A., Eds.; Wiley-VCH: New York, 1998. (b) Garrou, P. E.; Dubois, R. A.; Jung, C. W. *CHEMTECH* **1985**, *15*, 123. (c) Moser, W. R.; Papile, C. J.; Weininger, S. J. *J. Mol. Catal.* **1987**, *41*, 293. (d) Herrmann, W. A.; Brossmer, C.; Oefele, K.; Beller, M.; Fischer, H. *J. Organomet. Chem.* **1995**, *491*, C1.

(6) Albrecht, M. *Chem. Rev.* **2010**, *110*, 576, and references therein.

(7) Jones, W. D.; Feher, F. J. *J. Am. Chem. Soc.* **1985**, *107*, 620.

(8) (a) Muetterties, E. L.; Rhodin, T. N.; Band, E.; Brucker, C.; Pretzer, H. *Chem. Rev.* **1979**, *79*, 91. (b) Dyson, P. J. *Coord. Chem. Rev.* **2004**, *248*, 2443.

(9) (a) Clucas, J. A.; Foster, D. F.; Harding, M. M.; Smith, A. K. *Chem. Commun.* **1984**, 949. (b) Brown, M. P.; Dolby, P. A.; Harding, M. M.; Mathews, A. J.; Smith, A. K. *Dalton Trans.* **1993**, 1671.

(10) For selected reports employing $HOs_3(CO)_8$[μ-PhP(C_6H_4-μ_2,η^1)CH_2PPh_2] as a starting material in the synthesis of other polynuclear osmium clusters, see: (a) Clucas, J. A.; Harding, M. M.; Smith, A. K. *Chem. Commun.* **1985**, 1280. (b) Bartlett, R. A.; Cardin, C. J.; Cardin, D. J.; Lawless, G. A.; Power, J. M.; Power, P. P. *Chem. Commun.* **1988**, 312. (c) Brown, M. P.; Dolby, P. A.; Harding, M. M.; Mathews, A. J.; Smith, A. K.; Osella, D.; Arbrun, M.; Gobetto, R.; Raithby, P. R.; Zanello, P. *Dalton Trans.* **1993**, 827. (d) Abedin, S. M. T.; Hardcastle, K. I.; Kabir, S. E.; Malik, K. M. A.; Mottalib, M. A.; Rosenberg, E.; Abedin, M. J. *Organometallics* **2000**, *19*, 5623. (e) Deeming, A. J.; Hassan, M. M.; Kabir, S. E.; Nordlander, E.; Tocher, D. A. *Dalton Trans.* **2004**, 3709. (f) Kabir, S. E.; Miah, M. A.; Sarker, N. C.; Golzar-Hussain, G. M.; Hardcastle, K. I.; Nordlander, E.; Rosenberg, E. *Organometallics* **2005**, *24*, 3315. (g) Hassan, M. R.; Hogarth, G.; Golzar-Hossain, G. M.; Kabir, S. E.; Raha, A. K.; Saha, M. S.; Tocher, D. A. *Organometallics* **2007**, *26*, 6473.

(11) For a recent review that outlines the stabilizing role played by the dppm ligand in $M_3(CO)_{10}$(dppm) clusters (where M = Ru, Os), see: Kabir, S. E.; Hogarth, G. *Coord. Chem. Rev.* **2009**, *253*, 1285.

(12) (a) Adams, R. D.; Captain, B.; Fu, W.; Hall, M. B.; Smith, M. D.; Webster, C. E. *Inorg. Chem.* **2004**, *43*, 3921. (b) Adams, R. D.; Captain, B.; Hall, M. B.; Smith, J. L., Jr.; Webster, C. E. *J. Am. Chem. Soc.* **2005**, *127*, 1007. (c) Adams, R. D.; Captain, B.; Beddie, C.; Hall, M. B. *J. Am. Chem. Soc.* **2007**, *129*, 986. (d) Adams, R. D.; Captain, B.; Smith, M. D.; Beddie, C.; Hall, M. B. *J. Am. Chem. Soc.* **2007**, *129*, 5981. (e) Adams, R. D.; Boswell, E. M.; Hall, M. B.; Yang, X. *Organometallics* **2008**, *27*, 4938. (f) Adams, R. D.; Hall, M. B.; Pearl, W. C., Jr.; Yang, X. *Inorg. Chem.* **2009**, *48*, 652.

(13) (a) Kandala, S.; Hammons, C.; Watson, W. H.; Wang, X.; Richmond, M. G. *Dalton Trans.* **2010**, *39*, 1620. (b) Poola, B.; Carrano, C. J.; Richmond, M. G. *Organometallics* **2008**, *27*, 3018. (c) Watson, W. H.; Kandala, S.; Richmond, M. G. *J. Organomet. Chem.* **2007**, *692*, 1648; 968. (d) Kandala, S.; Richmond, M. G. *Inorg. Chem.* **2006**, *45*, 5976. (e) Watson, W. H.; Wu, G.; Richmond, M. G. *Organometallics* **2005**, *24*, 5431. (f) Bott, S. G.; Shen, H.; Richmond, M. G. *J. Organomet. Chem.* **2004**, *689*, 3426. (g) Bott, S. G.; Shen, H.; Senter, R. A.; Richmond, M. G. *Organometallics* **2003**, *22*, 1953. (h) Bott, S. G.; Yang, K.; Talafuse, K. A.; Richmond, M. G. *Organometallics* **2003**, *22*, 1383.

(14) Watson, W. H.; Wu, G.; Richmond, M. G. *Organometallics* **2006**, *25*, 930.

Scheme 1

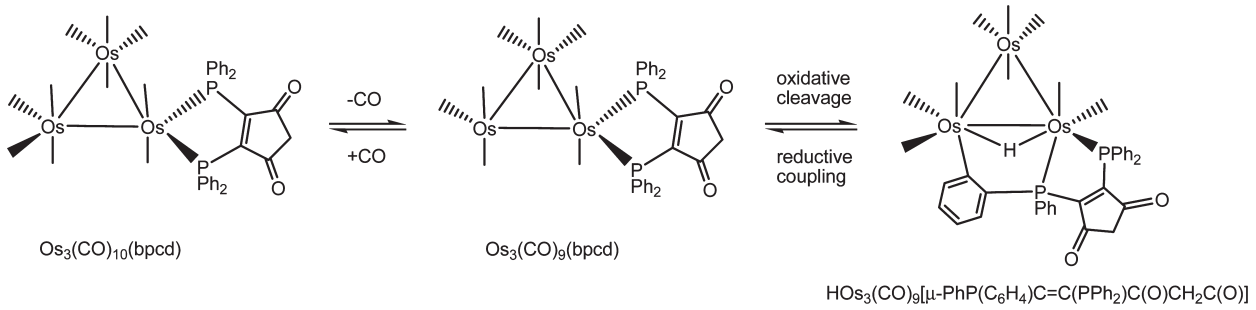

and establishes the reversible nature associated with the reactivity of the C−H bond in terms of oxidative cleavage and reductive coupling steps. On the basis of kinetic and isotopic substitution studies on the reductive coupling step, we have confirmed that C−H bond formation exhibits an inverse equilibrium isotope effect (EIE). These data strongly support the intermediacy of the transient π-complex $Os_3(CO)_9[\mu$-$PhP(\mu$-$C_6H_5)C{=}C(PPh_2)C(O)CH_2C(O)]$, whose formation precedes the generation of the coordinatively unsaturated cluster $Os_3(CO)_9$(bpcd). Scheme 1 illustrates this particular reaction.

Notwithstanding the fact that the activation of the dppm ligand in $Os_3(CO)_{10}$(dppm) is facile and reversible and that $HOs_3(CO)_8[\mu$-$PhP(C_6H_4$-$\mu_2,\eta^1)CH_2PPh_2]$ serves as a cluster synthon for "$Os_3(CO)_8$(dppm)", no mechanistic data exist for any of the steps associated with this transformation aside from empirical product distributions based on ligand substitution studies that have employed these two clusters.[10c−e,15,16] The unanswered questions concerning the oxidative cleavage and reductive coupling steps attendant in the activation of the dppm ligand in $Os_3(CO)_{10}$(dppm) and $HOs_3(CO)_8[\mu$-$PhP(C_6H_4$-$\mu_2,\eta^1)CH_2PPh_2]$ require resolution before generalities involving the ortho metalation in different $Os_3(CO)_{10}$(diphosphine) clusters can be made with certainty. Moreover, knowledge of such ligand activation is required if these and related cluster systems are to be exploited in any catalysis scenario. In the present work, we report our kinetic and isotope studies on the ortho metalation of the bridging diphosphine ligand in $Os_3(CO)_{10}$(dppm), and the results from this study are contrasted with the ortho-metalation data obtained from $Os_3(CO)_{10}$(bpcd). DFT calculations have also been performed in order to shed insight on the intermediates in this reaction and to facilitate the construction of a working mechanism that is consistent with the experimental results.

(15) To our knowledge, only one kinetic study on $Os_3(CO)_{10}$(dppm) exists, and this involves the kinetic measurement for the ring closure of the dppm ligand in $Os_3(CO)_{11}(\eta^1$-dppm): Poë, A.; Sekhar, V. C. *J. Am. Chem. Soc.* **1984**, *106*, 5034.

(16) (a) Raha, A. K.; Ghosh, S.; Manzurul Karim, M.; Tocher, D. A.; Begum, N.; Sharmin, A.; Rosenberg, E.; Kabir, S. E. *J. Organomet. Chem.* **2008**, *693*, 3613. (b) Azad, S. M.; Azam, K. A.; Kabir, S. E.; Saha, M. S.; Golzar Hossain, G. M. *J. Organomet. Chem.* **2005**, *690*, 4206. (c) Abedin, S. M. T.; Azam, K. A.; Hursthouse, M. B.; Kabir, S. E.; Malik, K. M. A.; Mottalib, M. A.; Rosenberg, E. *J. Cluster Sci.* **2001**, *12*, 5. (d) Kabir, S. E.; Abdul Malik, K. M.; Molla, E.; Abdul Mottalib, M. *J. Organomet. Chem.* **2000**, *616*, 157. (e) Azam, K. A.; Hursthouse, M. B.; Islam, M. R.; Kabir, S. E.; Malik, K. M. A.; Miah, R.; Sudbrake, C.; Vahrenkamp, H. *Dalton Trans.* **1998**, 1097. (f) Bruce, M. I.; Horn, E.; Bin Shawkataly, O.; Snow, M. R.; Tiekink, E. R. T.; Williams, M. L. *J. Organomet. Chem.* **1986**, *316*, 187. (g) Cartwright, S.; Clucas, J. A.; Dawson, R. H.; Foster, D. F.; Harding, M. M.; Smith, A. K. *J. Organomet. Chem.* **1986**, *302*, 403.

Experimental Section

General Methods. The $Os_3(CO)_{10}$(dppm) cluster was prepared from the reaction of dppm with either $Os_3(CO)_{12}$ or $Os_3(CO)_{10}(MeCN)_2$, the latter which was synthesized from $Os_3(CO)_{12}$, Me_3NO, and MeCN.[17] The parent cluster $Os_3(CO)_{12}$ was prepared from OsO_4 and CO.[18] The OsO_4 was purchased from Engelhard Chemical Co., and the chemicals dppm, 2-bromoaniline, 2,6-dibromoaniline, diphenylacetic acid, BuLi (2.5 M in hexanes), and $Me_3NO\cdot xH_2O$ were purchased from Aldrich Chemical Co. The anhydrous Me_3NO employed in our studies was obtained from $Me_3NO\cdot xH_2O$, after the waters of hydration were azeotropically removed under reflux using benzene as a solvent. The deuterated compounds D_2O (99.5% D), NaOD (40% in D_2O; 99.5% D), benzene-d_6 (99.6% D), toluene-d_8 (99.6% D), CD_2Cl_2 (99.8% D), $CDCl_3$ (99.8% D), and MeOD (99.8% D) were purchased from Cambridge Isotope Laboratories. All reaction solvents were distilled from a suitable drying agent under argon or obtained from an Innovative Technology solvent purification system; when not in use, the purified solvents were stored in Schlenk storage vessels equipped with high-vacuum Teflon stopcocks.[19] The NMR solvents benzene-d_6 and toluene-d_8 were purified by bulb-to-bulb distillation from Na/benzophenone, with the CD_2Cl_2 and $CDCl_3$ solvents distilled from P_2O_5. The molarity of the BuLi used in our reactions was periodically checked by titration against diphenylacetic acid.[20] The photochemical studies were conducted with an Oriel universal power supply equipped with a 200 W high-pressure Hg lamp. The quartz NMR tubes used in these studies were equipped with a high-vacuum stopcock, and the low-temperature UV photolysis experiments were carried out in a homemade Dewar constructed from Suprasil quartz tubing.

IR spectra were recorded on Nicolet 20SXB or 6700 FT-IR spectrometers in sealed 0.1 mm NaCl cells. The quoted ^1H, ^{13}C, and ^{31}P NMR data were recorded on a Varian VXR-500 spectrometer at 500, 125, and 202 MHz, respectively. The ^1H and ^{13}C spectral data have been referenced against the residue protiated and carbon resonance(s) of the NMR solvent. The reported ^{31}P chemical shift data were recorded in the proton-decoupled mode and are referenced to external H_3PO_4 (85%), whose chemical shift was set at $\delta = 0$. The GC-MS mass spectral data for the samples 2-deuterio-iodobenzene, 2,6-dideuterio-iodobenzene, PPh_3-d_{6ortho} and PPh_3-d_{3ortho} were recorded on a Finnigan/Thermo-Electron GC-MS system, while the ESI-MS spectra of the dppm isotopomers and their corresponding triosmium clusters were recorded on a Thermo Finnigan Deca XP ion trap mass spectrometer using 1% AcOH in MeCN or MeCN/KI as the sample matrix.

Preparation of dppm-d_{8ortho}. To 50 mL of liquid ammonia in a 100 mL Schlenk flask under argon at −78 °C was added 0.69 g

(17) Nicholls, J. N.; Vargas, M. D. *Inorg. Synth.* **1989**, *26*, 289.

(18) Drake, S. R.; Loveday, P. A. *Inorg. Synth.* **1990**, *28*, 230.

(19) Shriver, D. F. *The Manipulation of Air-Sensitive Compounds*; McGraw-Hill: New York, 1969.

(20) Kofron, W. G.; Baclawski, L. M. *J. Org. Chem.* **1976**, *41*, 1879.

(30 mmol) of sodium. The solution was stirred for several minutes prior to the addition of 4.0 g (15 mmol) of PPh_3-d_{6ortho}, at which time the initially blue solution slowly turned dark orange. After stirring for 0.5 h at −78 °C, 0.80 g (15 mmol) of NH_4Cl was added in one portion to quench the generated phenyl sodium from the reduction reaction. Stirring was continued for 1 h at −78 °C, and the orange solution was then treated with 0.48 mL (7.5 mmol) of CH_2Cl_2 in 2 mL of Et_2O to give a pale yellow solution that signaled the consumption of the sodium diphenylphosphide. The ammonia was allowed to evaporate, and 50 mL of degassed water was added to the remaining residue, followed by extraction of the aqueous layer with Et_2O (3 × 50 mL). The combined organic layers were dried over $MgSO_4$, after which the solution was filtered and then concentrated to dryness to afford the crude dppm-d_{8ortho}. The product was purified by flash-column chromatography over silica gel using CH_2Cl_2/hexane (3:7) to give dppm-d_{8ortho} as a colorless solid in 70% yield (2.1 g). ^{1}H NMR (C_6D_6): δ 2.78 (t, 2H, methylene, J_{PH} = 2.0 Hz), 7.04 (s, 12H, meta and para). ^{31}P NMR (C_6D_6): δ −23.21.[21] ESI-MS: m/z 393.47 $[M + H]^+$.

Synthesis of $Os_3(CO)_{10}$(dppm-d_{8ortho}). To a large Schlenk tube containing 0.46 g (0.49 mmol) of $Os_3(CO)_{10}(MeCN)_2$ was added 100 mL of CH_2Cl_2 via cannula, followed by 0.20 g (0.51 mmol) of dppm-d_{8ortho}. The solution was stirred for 12 h at room temperature and then examined by TLC, which confirmed the presence of the desired product. $Os_3(CO)_{10}$(dppm-d_{8ortho}) was subsequently purified by column chromatography over silica gel using a 3:7 mixture of CH_2Cl_2/hexane as the mobile phase. Recrystallization of the isolated product using benzene furnished 0.42 g (68%) of orange $Os_3(CO)_{10}$(dppm-d_{8ortho}). ^{1}H NMR (C_6D_6): δ 4.85 (t, 2H, methylene, J_{PH} = 10.5 Hz), 6.89 (s, 12H, meta and para). ^{31}P NMR (C_6D_6): δ −28.14. ESI-MS: m/z 1286.73 $[M + K]^+$ and 1258.92 $[M - CO + K]^+$.

Synthesis of $DOs_3(CO)_8[\mu$-(Ph-d_{2ortho})P(C_6H_3D-μ_2,η^1)CH_2-PPh_2-$d_{4ortho}]$ from $Os_3(CO)_{10}$(dppm-d_{8ortho}). To a 100 mL Schlenk tube under argon flush was charged 0.20 g (0.16 mmol) of $Os_3(CO)_{10}$(dppm-d_{8ortho}) and 50 mL of toluene. The solution was heated at reflux for 8 h, during which time the solution color gradually changed from orange to green as the octacarbonyl product formed. The solution was allowed to cool and the product isolated by column chromatography to give 0.13 g (68%) of $DOs_3(CO)_8[\mu$-(Ph-d_{2ortho})P(C_6H_3D-μ_2,η^1)CH_2PPh_2-$d_{4ortho}]$. ^{1}H NMR (C_6D_6): δ 3.96 (ddd, 1H, methylene, $^2J_{HH}$ = 14.1 Hz, $^3J_{PH}$ = 11.0, 6.3 Hz), 4.65 (ddd, 1H, methylene, $^2J_{HH}$ = 14.1 Hz, $^3J_{PH}$ = 11.1, 8.4 Hz), 6.24 (dt, H_b, $^3J_{HH}$ = 7.2 Hz from coupling with H_a and H_c, $^5J_{PH}$ = 2.2 Hz), 6.73−6.81 (m, 2H), 6.95−7.06 (m, 2H), 7.08−7.15 (m, H_c and 5H), 9.02 (ddd, H_a, $^3J_{HH}$ = 7.2 Hz from coupling with H_b, $^4J_{HH}$ = 1.3 Hz from coupling with H_c, $^4J_{PH}$ = 2.0 Hz).[22] ^{31}P NMR (C_6D_6): δ −19.82 (d, J_{PP} = 69 Hz), −18.67 (d, J_{PP} = 69 Hz). ESI-MS: m/z 1190.9 $[M]^+$ and m/z peaks for the consecutive loss of 1−7 CO groups.

Synthesis of $DOs_3(CO)_9[\mu$-(Ph-d_{2ortho})P(C_6H_3D)CH_2PPh_2-$d_{4ortho}]$ from $DOs_3(CO)_8[\mu$-(Ph-d_{2ortho})P(C_6H_3D-μ_2,η^1)CH_2-PPh_2-$d_{4ortho}]$ and CO. To 0.10 g (0.084 mmol) of $DOs_3(CO)_8$-$[\mu$-(Ph-d_{2ortho})P(C_6H_3D-μ_2,η^1)CH_2PPh_2-$d_{4ortho}]$ in a medium Schlenk tube was added 40 mL of toluene via syringe, after which the solution was cooled to ca. 5 °C. CO was slowly bubbled into the toluene solution for a period of 1 h, at which time TLC analysis revealed the complete consumption of the starting cluster and the presence of the nonacarbonyl product DOs_3-$(CO)_9[\mu$-(Ph-d_{2ortho})P(C_6H_3D)CH_2PPh_2-$d_{4ortho}]$. The solvent was removed under vacuum and the residue purified by flash-column chromatography over silica gel using a 7:3 mixture of CH_2Cl_2/hexane as the eluent. Yield: 97 mg (95%). ^{1}H NMR (C_6D_6): δ 3.39 (ddd, 1H, methylene, $^2J_{HH}$ = 12.4 Hz, $^3J_{PH}$ = 10.2, 9.2 Hz), 4.91 (ddd, 1H, methylene, $^2J_{HH}$ = 12.4 Hz, $^3J_{PH}$ = 12.7, 9.2 Hz), 6.02 (ddd, H_c, $^3J_{HH}$ = 7.3 Hz from coupling with H_b, $^3J_{HH}$ = 2.9 Hz from coupling with H_a, $^4J_{PH}$ = 1.0 Hz), 6.42 (dt, H_b, $^3J_{HH}$ = 7.3 Hz from coupling with H_a and H_c, $^5J_{PH}$ = 2.5 Hz), 6.65 (m, 2H), 6.74 (m, 1H), 6.83−7.09 (m, 6H), 8.20 (ddd, H_a, $^3J_{HH}$ = 7.3 Hz from coupling with H_b, $^4J_{HH}$ = 2.9 Hz from coupling with H_c, $^4J_{PH}$ = 1.2 Hz). ^{31}P NMR (C_6D_6): δ −23.23 (d, J_{PP} = 71 Hz), −14.21 (d, J_{PP} = 71 Hz). ESI-MS: m/z 1223.9 $[M - CO + 2H_2O]^+$.

Preparation of dppm-d_{4ortho}. To 50 mL of liquid ammonia in a 100 mL Schlenk flask under argon at −78 °C was added 0.60 g (26 mmol) of sodium, and stirring continued for 0.5 h before the addition of 3.5 g (13 mmol) of PPh_3-d_{3ortho}. The solution was stirred for an additional 0.5 h at −78 °C and then treated with 0.69 g (13 mmol) of NH_4Cl. At this point, 0.42 mL (6.5 mmol) of CH_2Cl_2 in 3 mL of Et_2O was added to the ammonia solution dropwise, and the solution was allowed to warm to room temperature with slow warming. The ammonia was allowed to evaporate and the crude product isolated upon a preliminary extractive workup. The dppm-d_{4ortho} was purified by flash-column chromatography over silica gel using a CH_2Cl_2/hexane (3:7) as a colorless solid in 75% yield (1.9 g). ^{1}H NMR (C_6D_6): δ 2.79 (t, 2H, methylene, J_{PH} = 2.0 Hz), 7.05 (bs, 12H, meta and para), 7.44 (b, 4H, ortho). ^{31}P NMR (C_6D_6): δ −23.13. ESI-MS: m/z 389.40 $[M + H]^+$.

Synthesis of $Os_3(CO)_{10}$(dppm-d_{4ortho}). To 0.25 g (0.27 mmol) of $Os_3(CO)_{10}(MeCN)_2$ in 60 mL of CH_2Cl_2 in a Schlenk flask was added 0.10 g (0.26 mmol) of dppm-d_{4ortho}. The solution was allowed to stir overnight, after which time the solvent was removed and the residue purified by flash-column chromatography. Recrystallization of the crude product using benzene afforded 0.23 g (72%) of orange $Os_3(CO)_{10}$(dppm-d_{4ortho}). ^{1}H NMR (C_6D_6): δ 4.86 (t, 2H, methylene, J_{PH} = 10.8 Hz), 6.90 (bs, 12H, meta and para), 7.26 (bs, 4H, ortho). ^{31}P NMR (C_6D_6): δ −27.10. ESI-MS: m/z 1282.93 $[M + K]^+$ and 1255.97 $[M - CO + K]^+$.

Carbonylation Kinetics. The UV−vis kinetic studies employing $HOs_3(CO)_{8,9}[\mu$-PhP(C_6H_4)$CH_2PPh_2]$ and $DOs_3(CO)_{8,9}$-$[\mu$-(Ph-d_{2ortho})P(C_6H_3D)CH_2PPh_2-$d_{4ortho}]$ were analyzed in Suprasil quartz UV−visible cells (1.0 cm width) that were equipped with a high-vacuum Teflon stopcock to facilitate handling on the vacuum line. The clusters $HOs_3(CO)_8[\mu$-PhP(C_6H_4-μ_2,η^1)$CH_2PPh_2]$ and $DOs_3(CO)_8[\mu$-(Ph-d_{2ortho})P(C_6H_3D-μ_2,η^1)-CH_2PPh_2-$d_{4ortho}]$ are extremely sensitive to added CO, and the samples were thermally equilibrated in the UV−vis cell holder

(21) Cf.: the ^{31}P chemical shift of dppm-d_0 at δ −22.91 recorded under identical conditions.

(22) The labeling scheme employed in the assignment of the hydrogens on the metalated aryl ring in the d_8 isotopomers of $DOs_3(CO)_8$-$[\mu$-(Ph-d_{2ortho})P(C_6H_3D-μ_2,η^1)CH_2PPh_2-$d_{4ortho}]$ and $DOs_3(CO)_9[\mu$-(Ph-d_{2ortho})P(C_6H_3D)CH_2PPh_2-$d_{4ortho}]$ is shown below. The reported coupling constants for the hydrogens on the metalated aryl ring were determined from spectral simulations using gNMR.

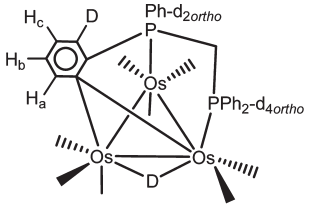

$DOs_3(CO)_8[\mu$-(Ph-d_{2ortho})P(C_6H_3D-μ_2,η^1)CH_2PPh_2-$d_{4ortho}]$

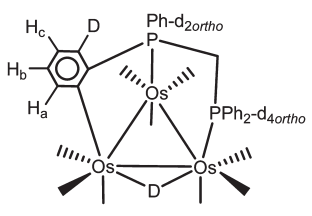

$DOs_3(CO)_9[\mu$-(Ph-d_{2ortho})P(C_6H_3D)CH_2PPh_2-$d_{4ortho}]$

Table 1. Experimental Rate Constants for the Carbonylation of $HOs_3(CO)_8[\mu\text{-}PhP(C_6H_4\text{-}\mu_2,\eta^1)CH_2PPh_2]$ to $HOs_3(CO)_9[\mu\text{-}PhP(C_6H_4)CH_2PPh_2]$ in Toluene[a]

entry	temp (K)	CO pressure (atm)	$10^4 k_{obsd}$ (s^{-1})
1	288.1	1.0	5.30(3)
2	288.1	1.0	5.23(2)[b]
3	288.1	17.0	39.3(1)
4	288.1	34.0	64.1(3)
5	293.2	1.0	7.26(2)
6	301.5	1.0	13.2(5)
7	307.9	1.0	23.2(5)
8	316.2	1.0	40.3(8)

[a] The UV−vis kinetic data were collected using a ca. 10^{-4} M solution of $HOs_3(CO)_8[\mu\text{-}PhP(C_6H_4\text{-}\mu_2,\eta^1)CH_2PPh_2]$ by following the decrease in the absorbance of the 388 nm band, unless otherwise noted. [b] Reaction carried out using a ca. 10^{-3} M solution of $HOs_3(CO)_8[\mu\text{-}PhP(C_6H_4\text{-}\mu_2,\eta^1)CH_2PPh_2]$ by following the decrease in the absorbance of the 600 nm band.

Table 2. Experimental Rate Constants for the Carbonylation of $HOs_3(CO)_9[\mu\text{-}PhP(C_6H_4)CH_2PPh_2]$ to $Os_3(CO)_{10}$(dppm) in Toluene[a]

entry	temp (K)	CO pressure (atm)	$10^5 k$ (s^{-1})
1	317.2	1.0	4.38(7)
2	323.0	1.0	9.59(9)
3	328.5	1.0	20.5(3)
4	328.5	17.0	16.8(3)
5	328.5	34.0	23.2(6)
6	334.0	1.0	31.3(4)
7	339.8	1.0	69(6)

[a] The UV−vis kinetic data were collected using a 8.73×10^{-3} M solution of $HOs_3(CO)_8[\mu\text{-}PhP(C_6H_4)CH_2PPh_2]$ by following the increase in the absorbance of either the 358 or 425 nm bands.

prior to the admission of CO. For those reactions involving the octacarbonyl cluster conducted under 1 atm of CO, the CO was administered directly into the reaction solution via a gastight syringe. In the case of $HOs_3(CO)_9[\mu\text{-}PhP(C_6H_4)CH_2PPh_2]$ and $DOs_3(CO)_9[\mu\text{-}(Ph\text{-}d_{2ortho})P(C_6H_3D)CH_2PPh_2\text{-}d_{4ortho}]$, the reaction solutions were purged with CO at room temperature immediately before the start of each kinetic experiment. The experiments performed under high CO pressure were carried out in a carbon-steel 300 mL autoclave, with the internal CO pressure regulated with the aid of a Tescom pressure regulator. The autoclave was equipped with a tip tube that enabled sample removal for UV−vis analysis while maintaining constant CO pressure. The Hewlett-Packard 8452A diode array spectrometer employed in our studies was configured with a custom VT cell holder, which was connected to a VWR constant-temperature circulator. The quoted reaction temperatures are considered to be accurate to within ±0.5 K. The UV−vis kinetics performed under 1 atm of CO were monitored by following the optical changes of the 388 or 600 nm band of the octacarbonyl cluster (decay) and the 358 or 425 nm band of the nonacarbonyl cluster (growth) as a function of time for at least 4−6 half-lives, while those reactions carried out under higher CO pressure were examined out to 3 half-lives. The UV−vis-derived rate constants quoted in Tables 1 and 2 were determined by nonlinear regression analysis using a single exponential function, with the initial (A_o) and final (A_∞) absorbance values and the rate constant (k) treated as free variables in the calculation.[23]

The quoted activation parameters for the conversion of $HOs_3(CO)_9[\mu\text{-}PhP(C_6H_4)CH_2PPh_2]$ to $Os_3(CO)_{10}$(dppm) were calculated from a plot of $\ln(k/T)$ versus T^{-1},[24] with the error limits representing the deviation of the data points about the least-squares line of the Eyring plot.

Computational Methodology and Modeling Details. All initial calculations were performed with the hybrid DFT functional B3LYP as implemented in the Gaussian 03 programming package.[25] This functional utilizes the Becke three-parameter exchange functional (B3)[26] combined with the correlation functional of Lee, Yang, and Parr (LYP)[27] and is known to produce good descriptions of reaction profiles for transition metal containing compounds.[28,29] The Os atoms were described using the LANL2DZ effective core potential (ecp) and basis set of Hay and Wadt[30] with the 6p orbitals replaced with the split valence functions from Couty and Hall.[31] The P atoms were described using the LANL2DZ(d) ecp basis set.[32,33] All other atoms (C, H, O) were modeled using a Pople style[34] double-ζ 6-31G-(d′,p′) basis set with polarization functions optimized for heavy atoms.[35]

All geometries were fully optimized and evaluated for the correct number of imaginary frequencies through calculation of the vibrational frequencies using the analytical Hessian. Zero imaginary frequencies (positive eigenvalues) correspond to an intermediate or local minimum, whereas one imaginary frequency designates a transition state. From the analytical Hessian zero-point energies as well as enthalpy and entropy corrections for 298.15 K were also calculated and added to the total electronic energy to obtain a total free energy, ΔG [298.15].

Implicit solvent effects were incorporated by using the polarizable continuum model[36] with toluene as the solvent using the parameter $\varepsilon = 2.379$. For this method we chose to employ the radii optimized for COSMO-RS by Klamt et al.[37] These radii were found to provide good results for systems involving hydrogen atom transfer. The solvent effects were calculated at geometries calculated in the gas phase. The resulting solvation free energy correction was added to the total free energy from above to obtain the total free energy.

Standard-state corrections were added to all species to convert concentrations from 1 atm to 1 M. This was accomplished via the equation $\Delta G^{\circ\prime} = \Delta G^\circ + RT\ln(Q^{\circ\prime}/Q^\circ)$, where the initial concentration $Q^\circ = 1$ atm (1/24.5 M for an ideal gas) and the final concentration $Q^{\circ\prime} = 1$ M.[38] Thus, a value of ca. −1.894 kcal/mol was added to the total free energy for each species. The overall effect of this correction is the addition of $(M - N) \times 1.894$ kcal/mol for the conversion of M molecules to N molecules. This approximation is added in order to better model the

(23) The rate calculations were performed by using the equation $A(t) = A_\infty + \Delta A e^{(-kt)}$ with the aid of the commercially available program Excel or Origin6.0.

(24) Carpenter, B. K. *Determination of Organic Reaction Mechanisms*; Wiley-Interscience: New York, 1984.

(25) Frisch, M. J.; et al. *Gaussian 03*, Revision E.01; Gaussian, Inc.: Pittsburgh, PA, 2003.
(26) Becke, A. D. *J. Chem. Phys.* **1993**, *98*, 5648.
(27) Lee, C.; Yang, W.; Parr, R. G. *Phys. Rev. B* **1988**, *37*, 785.
(28) Baker, J.; Muir, M.; Andzelm, J.; Scheiner, A. In *Chemical Applications of Density-Functional Theory*; Laird, B. B.; Ross, R. B.; Ziegler, T., Eds.; ACS Symposium Series 629; American Chemical Society: Washington, DC, 1996.
(29) Niu, S.; Hall, M. B. *Chem. Rev.* **2000**, *100*, 353.
(30) Hay, P. J.; Wadt, W. R. *J. Chem. Phys.* **1985**, *82*, 299.
(31) Couty, M.; Hall, M. B. *J. Comput. Chem.* **1996**, *17*, 1359.
(32) Höllwarth, A.; Böhme, M.; Dapprich, S.; Ehlers, A. W.; Gobbi, A.; Jonas, V.; Köhler, K. F.; Stegmann, R.; Veldkamp, A.; Frenking, G. *Chem. Phys. Lett.* **1993**, *208*, 237.
(33) Wadt, W. R.; Hay, P. J. *J. Chem. Phys.* **1985**, *82*, 284.
(34) (a) Hariharan, P. C.; Pople, J. A. *Chem. Phys. Lett.* **1972**, *16*, 217. (b) Francl, M. M.; Pietro, W. J.; Hehre, W. J.; Binkley, J. S.; Gordon, M. S.; DeFrees, D. J.; Pople, J. A. *J. Chem. Phys.* **1982**, *77*, 3654.
(35) Krishnan, R.; Binkley, J. S.; Seeger, R.; Pople, J. A. *J. Chem. Phys.* **1980**, *72*, 650.
(36) Tomasi, J.; Mennucci, B.; Cammi, R. *Chem. Rev.* **2005**, *105*, 2999.
(37) Klamt, A.; Jonas, V.; Buerger, T.; Lohrenz, J. C. W. *J. Chem. Phys.* **1998**, *102*, 5074.
(38) Cramer, C. J. *Essentials of Computational Chemistry*, 2nd ed.; Wiley: Chichester, UK, 2004; pp 378−379.

changes in solvent phase translational entropy when there are changes in the number of molecules present.

Kinetic isotope effects (KIE) were examined through calculation of the analytic Hessian upon substitution of deuterium for hydrogen. The new zero-point energies and enthalpy and entropy terms for the deuterated species were thus determined and used to obtain the corresponding free energies. The approximated KIEs were then calculated from $k_H/k_D = e^{(\Delta G_D - \Delta G_H/RT)}$.

Results and Discussion

I. Carbonylation Kinetics for the Conversion of $HOs_3(CO)_8[\mu\text{-PhP}(C_6H_4\text{-}\mu_2,\eta^1)CH_2PPh_2]$ to $HOs_3(CO)_9[\mu\text{-PhP}(C_6H_4)CH_2PPh_2]$. Thermolysis of $Os_3(CO)_{10}$(dppm) in refluxing toluene leads to CO loss and the formation of $HOs_3(CO)_9[\mu\text{-PhP}(C_6H_4)CH_2PPh_2]$, the latter presumably from the putative unsaturated cluster $Os_3(CO)_9$(dppm), which serves as the platform for the observed ortho-metalated product. $HOs_3(CO)_9[\mu\text{-PhP}(C_6H_4)CH_2PPh_2]$ is not stable under the reaction conditions and readily loses CO to afford the dimetalated cluster $HOs_3(CO)_8[\mu\text{-PhP}(C_6H_4\text{-}\mu_2,\eta^1)CH_2PPh_2]$. Our initial attempts to measure the rate of CO loss from $Os_3(CO)_{10}$(dppm) and $HOs_3(CO)_9[\mu\text{-PhP}(C_6H_4)CH_2PPh_2]$ were complicated by the fact that the cluster products from decarbonylation are extremely sensitive to the liberated CO in solution, leading us to question the validity of our computed rate constants. While we could measure the rate of disappearance of $Os_3(CO)_{10}$(dppm) and $HOs_3(CO)_9[\mu\text{-PhP}(C_6H_4)CH_2PPh_2]$ in solution by IR or UV−vis spectroscopy, we could not guarantee the absence of a back reaction between the liberated CO and the resulting decarbonylation product. Under these conditions the determined rate constants serve as a lower limit for the true loss of CO from the starting cluster. Control experiments conducted under CO (1 atm) confirmed our suspicions regarding the sensitivity of the decarbonylation products from $Os_3(CO)_{10}$(dppm) and $HOs_3(CO)_9[\mu\text{-PhP}(C_6H_4)CH_2PPh_2]$ to extraneous CO. Heating $Os_3(CO)_{10}$(dppm) under CO led to no perceptible spectral changes when monitored by IR spectroscopy, while $HOs_3(CO)_9[\mu\text{-PhP}(C_6H_4)CH_2PPh_2]$ reacted with CO to afford $Os_3(CO)_{10}$(dppm) in essentially quantitative yield.

The above limitations were circumvented by carrying out the carbonylation studies starting from the clusters $HOs_3(CO)_{8,9}[\mu\text{-PhP}(C_6H_4)CH_2PPh_2]$. The reaction between $HOs_3(CO)_8[\mu\text{-PhP}(C_6H_4\text{-}\mu_2,\eta^1)CH_2PPh_2]$ and excess CO proceeds rapidly in toluene to give $HOs_3(CO)_9[\mu\text{-PhP}(C_6H_4)CH_2PPh_2]$.[39] We would point out that no conversion of $HOs_3(CO)_9[\mu\text{-PhP}(C_6H_4)CH_2PPh_2]$ to $Os_3(CO)_{10}$(dppm) was observed under the time scale of these experiments. The progress of these reactions was conveniently monitored by following the decrease in the absorbance of the 388 nm band of the starting cluster. The pseudo-first-order rate constants for the first carbonylation step are listed in Table 1. As an independent check of the value of k_{obsd} measured at 388.1 K (entry 1) and the use of the 388 nm band of $HOs_3(CO)_8[\mu\text{-PhP}(C_6H_4\text{-}\mu_2,\eta^1)CH_2PPh_2]$ to accurately assess the progress of the reaction over the examined temperature range of 288−316 K, we also conducted one experiment using the weak visible band at 600 nm displayed by $HOs_3(CO)_8[\mu\text{-PhP}(C_6H_4\text{-}\mu_2,\eta^1)CH_2PPh_2]$ (entry 2).[40] The carbonylation

(39) The concentration of CO in toluene was determined by using the published solubility data. See: Basickos, L.; Bunn, A. G.; Wayland, B. B. *Can. J. Chem.* **2001**, *79*, 854.

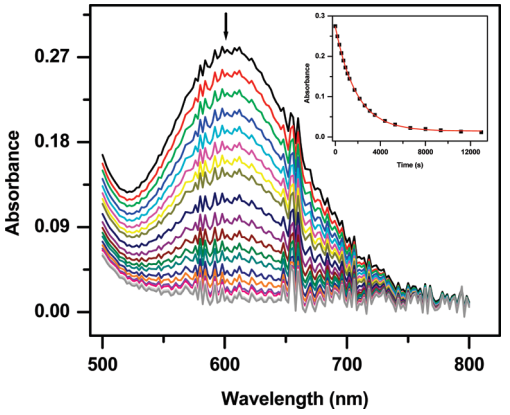

Figure 1. UV−vis spectral changes for $HOs_3(CO)_8[\mu\text{-PhP}(C_6H_4\text{-}\mu_2,\eta^1)CH_2PPh_2]$ in the presence of CO (1 atm) in toluene at 288.1 K. The inset shows the absorbance data versus time for the experimental data (■) and the nonlinear regression fit of the pseudo-first-order rate constant k_{obsd} (solid red line).

product is nonabsorbing at this wavelength, and this ensures that the measured rate of the reaction truly reflects the consumption of the $HOs_3(CO)_8[\mu\text{-PhP}(C_6H_4\text{-}\mu_2,\eta^1)CH_2PPh_2]$ cluster. Figure 1 shows the UV−vis spectral changes for the carbonylation reaction under 1 atm of CO and 288 K, with the inset depicting the least-squares fit of the rate constant (k_{obsd}) and the absorbance data.

The effect of CO on the reaction was investigated in more detail at 288 K. Entries 3 and 4, which represent reactions carried out at CO pressures of 17 and 34 atm, respectively, confirm that the rate is dependent on the [CO]. Graphical analysis of the 288 K data in terms of a plot of k_{obsd} versus [CO] (see Supporting Information) afforded a rate constant of $23.9(3) \times 10^{-3}$ M^{-1} s^{-1}. As mentioned earlier, the first carbonylation step proceeds rapidly, and attempts to measure the rate of the reaction at higher temperatures as a function of [CO] were deemed unfeasible using the conventional apparatus at our disposal.[41] The kinetic data are consistent with a reaction that is first-order in cluster and CO, and the rate-limiting step was initially assumed to involve the direct attack of CO on the cluster, coupled with the concerted conversion of the dimetalated aryl moiety to an η^1-aryl group. Equation 2 shows this transformation, where the rate law obeys the form

$$\text{rate} = k_1[\text{cluster}][\text{CO}]$$

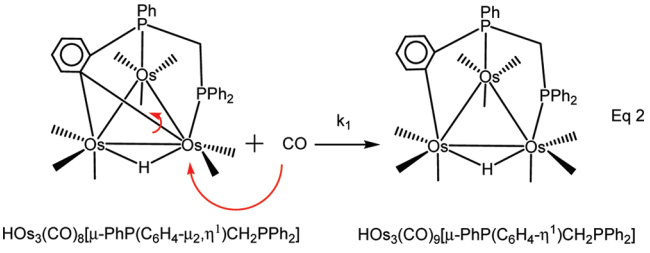

Eq 2

The simple nucleophilic addition of CO to the osmium center containing only two carbonyl groups depicted in eq 2 is kinetically valid provided the dimetalated phenyl moiety remains strongly tethered to both metals. However, if the aryl moiety is fluxional in terms of a reversible

Scheme 2

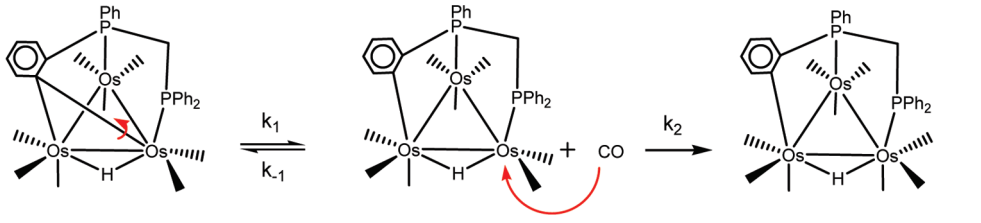

$HOs_3(CO)_8[\mu\text{-}PhP(C_6H_4\text{-}\mu_2,\eta^1)CH_2PPh_2]$ cluster A

$HOs_3(CO)_8[\mu\text{-}PhP(C_6H_4\text{-}\eta^1)CH_2PPh_2]$ cluster B

$HOs_3(CO)_9[\mu\text{-}PhP(C_6H_4)CH_2PPh_2]$ cluster C

$$\text{rate} = \frac{k_1k_2[A][CO]}{k_{-1} + k_2[CO]}$$

dissociation/coordination process with respect to the $Os(CO)_2$ center, this would lead to an enhanced exposure of the $Os(CO)_2$ center to CO attack in the "opened" cluster $HOs_3(CO)_8[\mu\text{-}PhP(C_6H_4\text{-}\eta^1)CH_2PPh_2]$. Such coordinative flexibility on the part of the metalated aryl moiety would be similar to the windshield wiper motion exhibited by nonclassical norbornyl cations and the migratory behavior of a wide variety of ligands in di- and polynuclear compounds.[42,43] Scheme 2 illustrates this scenario and shows the expected rate law for the capture of CO by $HOs_3(CO)_8[\mu\text{-}PhP(C_6H_4\text{-}\eta^1)CH_2PPh_2]$ (cluster B),[44] which is kinetically indistinguishable from the elementary second-order process depicted in eq 2. A distinction between the two mechanisms is possible based on the effect of [CO], provided saturation kinetics can be observed. Whereas the mechanism in eq 2 will always show a first-order dependence on [CO], steady-state considerations predict that the carbonylation will actually become independent of the attacking ligand at high concentrations of CO ($k_2[CO] \gg k_{-1}$). In the saturation regime, the reaction will reduce to a simple first-order reaction (rate = k_1[cluster A]). Unfortunately, this concept cannot be experimentally tested in the present case because the carbonylation is too rapid.

Increases in computing speed over the past decade have greatly facilitated the examination of complex metal cluster reactions by density functional theory (DFT). Several important studies have recently demonstrated the ability of DFT calculations to address multistep reaction mechanisms involving ligand fluxionality and substrate activation at different polynuclear ruthenium and osmium clusters.[45] Accordingly, we sought to resolve the above carbonylation conundrum in $HOs_3(CO)_8[\mu\text{-}PhP(C_6H_4\text{-}\mu_2,\eta^1)CH_2PPh_2]$ by means of DFT calculations, and here we initially optimized the structures of $HOs_3(CO)_8[\mu\text{-}PhP(C_6H_4\text{-}\mu_2,\eta^1)CH_2PPh_2]$ (**A1**) and $HOs_3(CO)_9[\mu\text{-}PhP(C_6H_4\text{-}\eta^1)CH_2PPh_2]$ (**B1**). The DFT-calculated structures for **A1** and **B1** are shown in Figure 2, with the computed structure of **A1** in good agreement with the X-ray diffraction structure.[9a] The bridging hydride in **A1**, which was not located during structural refinement, spans the Os−Os vector that also binds the metalated aryl moiety, as expected when the disposition of the ancillary CO groups are taken into account.[46] The computed versus experimentally measured Os−C bond distances of 2.38 Å [2.297(15) Å] and 2.33 Å [2.283(13) Å] associated with the aryl moiety that is bound to the $Os(CO)_3$ and $Os(CO)_2$ centers, respectively, confirm the metalation of this Os−Os vector. The computed structure of **B1** is in accord with the formulated structure for the nonacarbonyl cluster, especially with respect to the bond distances and angles exhibited by the metalated η^1-aryl moiety and the capping of the triangular Os_3 face by the 5*e* $PhP(C_6H_4)CH_2PPh_2$ donor ligand. Finally, **B1** compares well with the overall architecture exhibited by the structurally characterized derivative

(40) (a) The concentration of CO at 288 K may be estimated at ca. 8.0×10^{-3} M, leading to a CO/cluster ratio of ca. 8. While this ratio is slightly lower than that technically required for a reaction run under strict pseudo-first-order conditions (i.e., a 10-fold excess of ligand), it nonetheless gave a k_{obsd} value in excellent agreement with that reaction conducted under true pseudo-first-order conditions (entry 1). (b) For the kinetic treatment of different pseudo-first-order scenarios, see: Espenson, J. H. *Chemical Kinetics and Reaction Mechanisms*; McGraw-Hill: New York, 1995.

(41) The computed half-life of 4.3 min (17 atm CO) and 1.8 min (34 atm CO) for the two high-pressure carbonylations strongly support the need for stopped-flow techniques if one wishes to measure accurately the rate of the reaction at higher temperatures and CO pressure.

(42) For a general discussion on the properties and reactivity of norbornyl cations, see: March, J. *Advanced Organic Chemistry*, 4th ed.; Wiley: New York, 1992.

(43) For some representative organometallic examples involving the windshield wiper motion of ligands, see: (a) Huang, S.-H.; Watson, W. H.; Carrano, C. J.; Wang, X.; Richmond, M. G. *Organometallics* **2010**, *29*, 61. (b) Bergamo, M.; Beringhelli, T.; D'Alfonso, G.; Mercandelli, P.; Sironi, A. *J. Am. Chem. Soc.* **2002**, *124*, 5117. (c) Rosenberg, E.; Milone, L.; Gobetto, R.; Osella, D.; Hardcastle, K.; Hajela, S.; Moizeau, K.; Day, M.; Wolf, E.; Espitia, D. *Organometallics* **1997**, *16*, 2665. (d) Curtis, M. D.; Han, K. R.; Butler, W. M. *Inorg. Chem.* **1980**, *19*, 2096.

(44) The conversion of the dimetalated aryl group in $HOs_3(CO)_8[\mu\text{-}PhP(C_6H_4\text{-}\mu_2,\eta^1)CH_2PPh_2]$ to its η^1 isomer can theoretically occur at either osmium center that binds the metalated aryl group. This act will furnish two different osmium hinge or anchor points from which the η^1 isomer may transverse the original Os−Os vector. Given the steric congestion imposed about the face of the cluster by the axially disposed diphosphine ligand, only the η^1 isomer shown in Scheme 2 is regarded as feasible.

(45) (a) Persson, R.; Monari, M.; Gobetto, R.; Russo, A.; Aime, S.; Calhorda, M. J.; Nordlander, E. *Organometallics* **2001**, *20*, 4150. (b) Abdul Mottalib, M.; Begum, N.; Tareque Abedin, S. M.; Akter, T.; Kabir, S. E.; Arzu Miah, M.; Rokhsana, D.; Rosenberg, E.; Golzar Hossain, G. M.; Hardcastle, K. I. *Organometallic* **2005**, *24*, 4747. (c) Musaev, D. G.; Nowroozi-Isfahami, T.; Morokuma, K.; Rosenberg, E. *Organometallics* **2005**, *24*, 5973. (d) Musaev, D. G.; Nowroozi-Isfahami, T.; Morokuma, K.; Abedin, J.; Rosenberg, E.; Hardcastle, K. I. *Organometallics* **2006**, *25*, 203. (e) Cabeza, J. A.; Pérez-Carreño, E. *Organometallics* **2008**, *27*, 4697. (f) Cabeza, J. A.; del Río, I.; Fernández-Colinas, J. M.; Pérez-Carreño, E.; Sánchez-Vega, M. G.; Vázquez-García, D. *Organometallics* **2009**, *28*, 1832. (g) Cabeza, J. A.; Fernández-Colinas, J. F.; Pérez-Carreño, E. *Organometallics* **2009**, *28*, 4217. (h) Cabeza, J. A.; Van der Maelen, J. F.; García-Granda, S. *Organometallics* **2009**, *28*, 3666. (i) Cabeza, J. A.; del Río, I.; Goite, M. C.; Pérez-Carreño, E.; Pruneda, V. *Chem.—Eur. J.* **2009**, *15*, 7339.

(46) (a) Churchill, M. R.; Hollander, F. J.; Lashewycz, R. A.; Pearson, G. A.; Shapley, J. R. *J. Am. Chem. Soc.* **1981**, *103*, 2430. (b) Churchill, M. R.; Hollander, F. J. *Inorg. Chem.* **1981**, *20*, 4124.

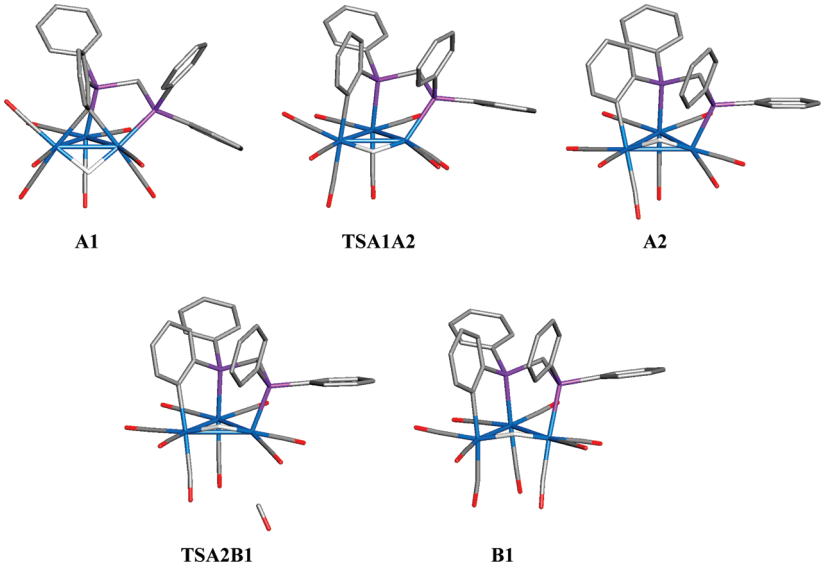

Figure 2. Optimized B3LYP structures for intermediates **A1**, **A2**, and **B1** and transition states **TSA1A2** and **TSA2B1**.

$HOs_3(CO)_8(PPr^i_3)[\mu\text{-}PhP(C_6H_4)CH_2PPh_2]$ that is obtained from the reaction of PPr^i_3 with $HOs_3(CO)_8[\mu\text{-}PhP(C_6H_4\text{-}\mu_2,\eta^1)CH_2PPh_2]$.[9b] Here the addition of the PPr^i_3 ligand to the cluster is accompanied by a formal opening of the metalated aryl moiety analogous to that expected for the carbonylation product $HOs_3(CO)_9[\mu\text{-}PhP(C_6H_4)CH_2PPh_2]$.

The direct addition of CO to the $Os(CO)_2$ center in **A1** that is opposite the face-capping diphosphine ligand seemed a promising route to **B1**. The incoming CO was allowed to approach the metal center with an axial-like trajectory, and a two-dimensional scan was performed with constraints on the cleavage of the Os−C(aryl) and the formation of the Os−CO bond distances. Results of the scan revealed a monotonic increase in the overall energy of the associative region (long Os−C(aryl) and short Os−CO distances) of the potential energy surface (PES) with no apparent saddle point and energies > 50 kcal/mol for the ΔE_{gas}. All attempts to find a concerted transition state in this process collapsed to product, reagents, or a third species resembling **B1** but with an unrealistically long $Os-CO_{new}$ bond distance. The dissociation or elongation of the Os−C(aryl) bond leading to the species $HOs_3(CO)_8[\mu\text{-}PhP(C_6H_4\text{-}\eta^1)CH_2PPh_2]$ was next examined, and the dissociative region of the PES (long Os−C(aryl) and $Os-CO_{new}$ distances) was found to be significantly lower in energy vis-à-vis the initial CO addition route examined. The geometry-optimized structure of $HOs_3(CO)_8[\mu\text{-}PhP(C_6H_4\text{-}\eta^1)CH_2PPh_2]$ is represented by species **A2**, and this closely resembles the structure of **B1** except for the missing CO group. The binding of the triangular metal face by the $PhP(C_6H_4)CH_2PPh_2$ ligand in **A2** is similar to the diphosphine ligand in $HOs_3(CO)_8(PPr^i_3)[\mu\text{-}PhP(C_6H_4)CH_2PPh_2]$.[9b] Moreover, elongation of the Os−C(aryl) vector from 2.33 Å (**A1**) to 3.99 Å (**A2**) exceeds the sum of the van der Waals radii of the carbon and osmium atoms, precluding any direct bonding between these centers.[47,48]

Figure 3 shows the free-energy profile for the conversion of **A1** to **B1**, along with the pertinent transition states

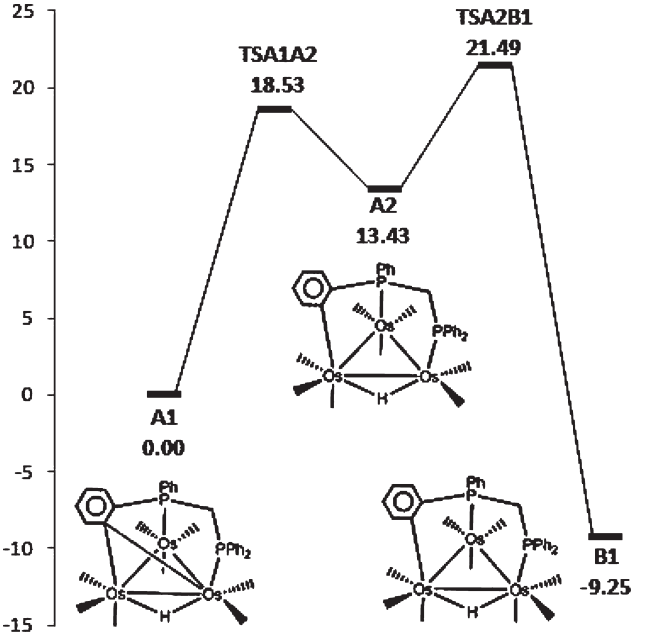

Figure 3. Free-energy profile for conversion of **A1** to **B1** in the presence of CO. Energy values are ΔG's in kcal/mol with respect to **A1**.

TSA1A2 and **TSA2B1**, whose optimized geometries are depicted in Figure 2. **TSA1A2** corresponds to the breaking of the Os−C(aryl) bond as the dimetalated aryl cluster transforms to the η^1 isomer. This transition state is fairly late and resembles species **A2** to a high degree. The nonbonding Os−C(aryl) bond distance of 3.43 Å in **TSA1A2** is significantly weakened relative to that distance found in **A1** and fully consistent with this process. The addition of CO to **A2** leads to **TSA2B1**, which corresponds to the high-energy point on the PES with a $\Delta G^{\ddagger}$ value of 21.5 kcal/mol relative to **A1**. **TSA2B1** is an early transition state and resembles **A2** with the distant CO moiety approaching the $Os(CO)_2$ moiety from the exposed polyhedral face of the cluster. That **TSA2B1** amounts to the rate-determining step for the overall process is in full harmony with the reaction kinetics and the sequence of events depicted in Scheme 2.[49]

(47) The opening of the dimetalated aryl group in $HOs_3(CO)_8[\mu\text{-}PhP(C_6H_4\text{-}\mu_2,\eta^1)CH_2PPh_2]$ that accompanies the addition of PPr^i_3 leads to a concomitant increase of the initial Os−C(aryl) bond distance of 2.28(1) Å to over 4.08 Å. See: ref 9b.

(48) Bondi, A. *J. Phys. Chem.* **1964**, *68*, 441.

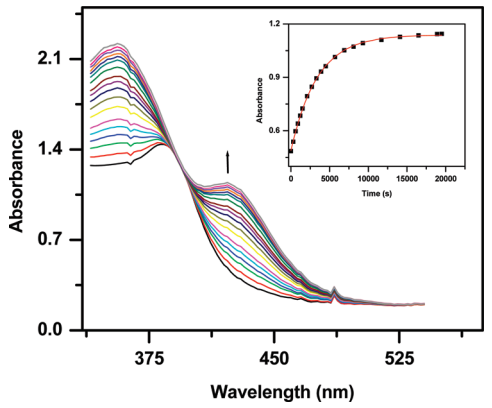

Figure 4. UV−vis spectral changes for $HOs_3(CO)_9[\mu$-PhP$(C_6H_4)CH_2PPh_2]$ in the presence of CO (1 atm) in toluene at 334.0 K. The inset shows the absorbance data versus time for the experimental data (■) and the nonlinear regression fit of the first-order rate constant k (solid red line).

II. Carbonylation Kinetics for the Conversion of $HOs_3(CO)_9[\mu$-PhP$(C_6H_4)CH_2PPh_2]$ to $Os_3(CO)_{10}$(dppm). The carbonylation reaction leading to $Os_3(CO)_{10}$(dppm), and with it the important reductive coupling step that regenerates the aryl C−H bond, proceeds cleanly and without the presence of spectroscopically observable intermediates in toluene over the temperature range 317−340 K. The kinetics were investigated by UV−vis spectroscopy under CO (excess) by following the increase in absorbance of the 358 or 425 nm band belonging to $Os_3(CO)_{10}$(dppm). Figure 4 shows the UV−vis spectral changes for the reaction of $HOs_3(CO)_9[\mu$-PhP$(C_6H_4)CH_2PPh_2]$ with CO at 334 K, while the inset reveals the least-squares fit of the first-order rate constant (k) as a function of the absorbance data. The first-order rate constants for these reactions are summarized in Table 2. Inspection of entries 3−5 confirms that the rate of the reaction is independent of added CO, and this supports a process that is first-order in starting cluster and consistent with the rate law

$$\text{rate} = k_1[\text{cluster}]$$

The Eyring activation parameters computed for the present carbonylation [$\Delta H^{\ddagger} = 24.5(6)$ kcal/mol and $\Delta S^{\ddagger} = -1(2)$ eu] are comparable to those data found by us in the conversion of $HOs_3(CO)_9[\mu$-PhP(C_6H_4)C=C(PPh_2)C(O)-CH_2C(O)] to $Os_3(CO)_{10}$(bpcd),[14,50] where compelling kinetic evidence was presented for the formation of an intermediate π-complex, prior to the rate-limiting release of the unsaturated cluster $Os_3(CO)_9$(bpcd) (see Scheme 1). We would also note that the activation parameters computed for $HOs_3(CO)_9[\mu$-PhP$(C_6H_4)CH_2PPh_2]$ are not unlike those values reported by Bergman for the reductive coupling of benzene from dinuclear compound $Cp^*_2Ir_2(Ph)(\mu$-H$)(\eta^1,\eta^3$-$C_3H_4)$, which presumably affords $Cp^*_2Ir_2(\eta^2$-benzene$)(\eta^1,\eta^3$-$C_3H_4)$ prior to the formation of the 32e species $Cp^*_2Ir_2(\eta^1,\eta^3$-$C_3H_4)$ in the rate-limiting step.[51]

III. Synthesis of dppm-d_{8ortho} and Deuterium Isotope Effects in the Carbonylation of $DOs_3(CO)_{8,9}[\mu$-(Ph-d_{2ortho})P-$(C_6H_3D)CH_2PPh_2$-$d_{4ortho}]$. The effect of deuterium on the reductive coupling step that accompanies the formation of $Os_3(CO)_{10}$(dppm) was investigated by using an isotopically substituted dppm ligand where all of the ortho hydrogens were replaced by deuterium atoms. The needed dppm-d_{8ortho} ligand was prepared according to the protocol outlined in Scheme 3, and the introduction of deuterium was made through a modification of the functional-group-directed reductive debromination described by Schlosser.[52,53] The undesirable incorporation of the original amine hydrogens into the ortho sites of the desired 2,6-dideuteroaniline during the reductive debromination was minimized by using 2,6-dibromoaniline-d_2.[54] The deuterium content at the ortho sites in 2,6-dideuteroaniline was found to be >98% isotopic purity by ^{1}H NMR, and this material was immediately diazotized and then converted to 2,6-dideutero-iodobenzene. The mass spectrum of the latter compound revealed a molecular ion two mass units greater than iodobenzene, and the ^{1}H and ^{13}C NMR properties were fully consistent with the formulated structure. Lithiation of 2,6-dideutero-iodobenzene, followed by treatment with PCl_3, gave PPh_3-d_{6ortho} in an overall yield of 30%. While PPh_3-d_{6ortho} may also be prepared through the metal-catalyzed deuteration of PPh_3 using D_2 gas,[55] our procedure lends itself to the large-scale synthesis of PPh_3-d_{6ortho}, eliminates the incomplete deuteration of the ortho sites, and avoids any degradation of the phosphine ligand through P−C bond cleavage. Finally, reductive cleavage of one of the P−Ph bonds in PPh_3-d_{6ortho} was best executed by using Na in liquid NH_3, followed by neutralization of the NaPh-d_{2ortho} with NH_4Cl and then addition of CH_2Cl_2, which furnished dppm-d_{8ortho}. The ^{1}H NMR spectrum of dppm-d_{8ortho} recorded in C_6D_6 showed no detectable *ortho* hydrogens, and the ESI mass spectrum showed a m/z peak at 393.47 for the species $[M + H]^+$.

The starting cluster $Os_3(CO)_{10}$(dppm-d_{8ortho}) was next prepared from $Os_3(CO)_{10}(MeCN)_2$ and dppm-d_{8ortho} in 68% yield. The isolated product was characterized by NMR and mass spectrometry, with the data in accord with the formulated structure. Controlled thermolysis of $Os_3(CO)_{10}$(dppm-d_{8ortho}) in toluene afforded the deuteride cluster $DOs_3(CO)_8[\mu$-(Ph-d_{2ortho})P$(C_6H_3D$-$\mu_2,\eta^1)CH_2PPh_2$-$d_{4ortho}]$, and this material was judged to be very pure by ^{1}H NMR spectroscopy, showing no evidence for the presence of ortho hydrogens or a bridging hydride ligand.[56] The absence of the latter ligand is important, as it allows us to eliminate a

(49) From the calculated energy differences in Figure 3, we estimate k_{-1}(**A2→TSA1A2**) and k_2(**A2→TSA1A2**) as ca. 1.8×10^{-4} s^{-1} and 1.2×10^{-6} s^{-1} M^{-1}, respectively. The rate differences reinforce our assumption concerning Scheme 2 and the fact that $k_{-1} \gg k_2$. Under the present conditions, the ligand-independent path for carbonylation would become competitive with the second-order process at [CO] > 150 M.

(50) Since the transformation of $HOs_3(CO)_9[\mu$-PhP$(C_6H_4)CH_2PPh_2]$ to $Os_3(CO)_{10}$(dppm) does not occur via a single elementary reaction, any mechanistic inference based solely on the activation parameters is best acknowledged tenuously.

(51) McGhee, W. D.; Hollander, F. J.; Bergman, R. G. *J. Am. Chem. Soc.* **1988**, *110*, 8428.

(52) Heiss, C.; Marzi, E.; Schlosser, M. *Eur. J. Org. Chem.* **2003**, 4625.

(53) For a comprehensive treatise on the use of organozinc and related organometallics in organic synthesis, see: *Organometallics in Synthesis: A Manual*, 2nd ed.; Schlosser, M., Ed.; Wiley: Chichester, England, 2002.

(54) Here the exchange of the original amino hydrogens by deuterium was achieved by treating 2,6-dibromoaniline with three separate 50 mL portions of MeOD. Each individual exchange reaction was stirred overnight, after which the solvent was removed and fresh MeOD added to the deuterium-enriched aniline. The ratio of deuterium:hydrogen in the first exchange cycle was ca. 15:1, and this ratio increases with each successive exchange cycle.

(55) Parshall, G. W.; Knoth, W. H.; Schunn, R. A. *J. Am. Chem. Soc.* **1969**, *91*, 4990.

(56) Cf.: the ^{1}H NMR spectrum of $HOs_3(CO)_8[\mu$-PhP$(C_6H_4$-$\mu_2,\eta^1)CH_2PPh_2]$ recorded in C_6D_6 under identical conditions.

Scheme 3

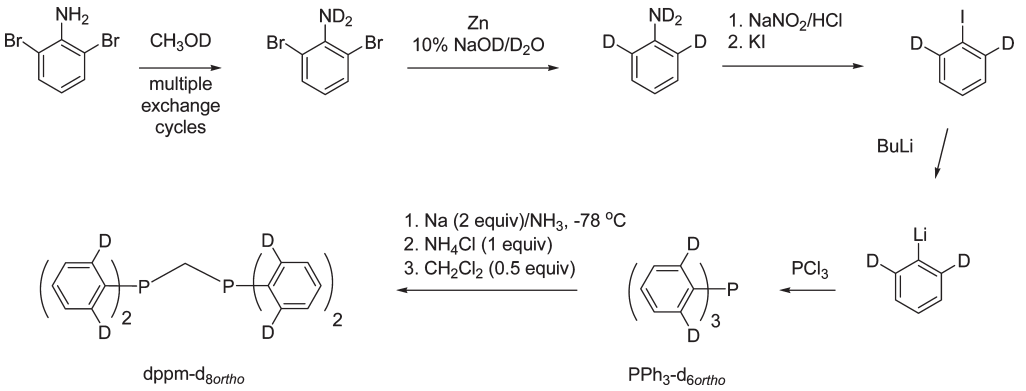

scenario involving the proton/deuteron exchange between the chromatographic support and the isotopically labeled cluster.[57,58] The carbonylation of $DOs_3(CO)_8[\mu$-(Ph-d_{2ortho})P-(C_6H_3D-μ_2,η^1)CH_2PPh_2-d_{4ortho}] to $DOs_3(CO)_9[\mu$-(Ph-d_{2ortho})-$P(C_6H_3D)CH_2PPh_2$-d_{4ortho}] was investigated at 288.1 K under 1 atm of CO in a manner identical to that employed for the protiated isotopomer. Two independent carbonlyations were conducted, and each displayed well-behaved pseudo-first-order decay curves for the starting cluster, from which the average k_{obsd} value of $5.16(2) \times 10^{-4}$ s^{-1} was computed.[59] This latter value compares well with the k_{obsd} value of $5.23(2) \times 10^{-4}$ s^{-1} from the d_0-isotopomer (Table 1) and confirms the absence of any significant isotope effect in the first carbonylation step. The insensitivity of the rate constants to isotopic substitution reinforces the carbonylation mechanism that is depicted in Scheme 2.

The carbonylation of $DOs_3(CO)_9[\mu$-(Ph-d_{2ortho})$P(C_6H_3D)$-CH_2PPh_2-d_{4ortho}] to $Os_3(CO)_{10}$(dppm-d_{8ortho}) was examined by UV−vis spectroscopy at 323.0 and 334.0 K under 1 atm of CO. The first-order rate constants of $19.1(2)$ e^{-5} s^{-1} (323 K) and $62.4(5) \times 10^{-5}$ s^{-1} (334 K) measured for the consumption of $DOs_3(CO)_9[\mu$-(Ph-d_{2ortho})$P(C_6H_3D)CH_2PPh_2$-d_{4ortho}] are faster than those reactions employing the d_0 isotopomer (Table 2), giving rise to an inverse isotope effect of 0.50 at both temperatures. The observed inverse isotope effect is readily understood in terms of a reductive coupling sequence that contains a preequilibrium that exhibits an inverse equilibrium isotope effect (EIE), followed by a slower rate-limiting step that is isotope insensitive (i.e., Kk).[2d,g,60,61] Using the deuterated isotopomer for illustrative purposes, the formation of the aryl C−D bond through reductive coupling would yield the preequilibrium species $Os_3(CO)_9[\mu$-(Ph-d_{2ortho})$P(C_6H_3D_2$-$\pi)CH_2PPh_2$-d_{4ortho}], whose aryl ring must remain bound to the cluster at the locus responsible for ortho metalation.[62] Such a multistep scenario is predicted to display an inverse EIE when the vibrational frequencies of the participant atoms are taken into account.[63] The transfer of the deuteride ligand from the osmium metal to the ortho carbon atom leads to a stronger aryl C−D bond relative to the osmium−deuteride bond in $DOs_3(CO)_9[\mu$-(Ph-d_{2ortho})P-$(C_6H_3D)CH_2PPh_2$-d_{4ortho}]. The faster reductive coupling experimentally found for the deuterated isotopomer stems from its greater preequilibrium concentration of $Os_3(CO)_9$-$[\mu$-(Ph-d_{2ortho})$P(C_6H_3D_2)CH_2PPh_2$-d_{4ortho}] relative to Os_3-$(CO)_9[\mu$-$PhP(C_6H_5)CH_2PPh_2]$.[64] Scheme 4 illustrates the reductive coupling reaction leading to $Os_3(CO)_9$(dppm-P_a,P_e) (where P_a = axial phosphine; P_e = equatorial phosphine). Not depicted in the scheme is the rapid isomerization of the dppm ligand and the trapping of CO by $Os_3(CO)_9$-(dppm-P_e,P_e) to give $Os_3(CO)_{10}$(dppm-P_e,P_e), which occur after the rate-limiting step involving the generation of Os_3-$(CO)_9$(dppm-P_a,P_e). Admittedly simplistic, the fundamentals at play in this scenario have been shown to be operative in the carbonylation of $HOs_3(CO)_9[\mu$-$PhP(C_6H_4)C{=}C$-$(PPh_2)C(O)CH_2C(O)]$ to $Os_3(CO)_{10}$(bpcd),[14] in addition to numerous mononuclear compounds that display a dissociative loss of an alkane and arene from hydrido(alkyl) and hydrido(aryl) precursors.[60,65] In the latter examples, transient metal-bound σ-alkane and π-arene species have been unequivocally demonstrated as active participants in the rate-limiting step.

IV. NMR Evidence for Low-Energy H/D Scrambling in Ortho Metalation. Additional experiments were conducted in order to establish the existence of a labile π-arene (or agostic C−H) compound as an intermediate that precedes ortho metalation on the reaction coordinate. Ideally, the testing of a putative π/agostic species may be achieved by studying the ortho-metalation step (i.e., oxidative coupling) under kinetically and thermodynamically controlled reaction conditions. Here valuable information may be gleaned concerning the

Scheme 4

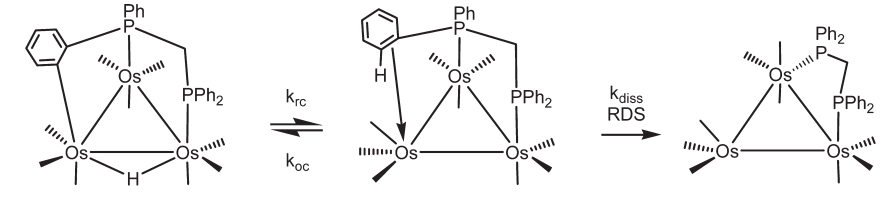

$$k_{obsd} = k_{rc}k_{diss}/k_{oc} = Kk_{diss}$$

discriminatory C−H versus C−D bond activation at the cluster. To this end, we have prepared the isotopically substituted ligand dppm-d_{4ortho}, whose ortho sites on each aryl ring contain one hydrogen and one deuterium relative to the phosphorus atom. Starting from 2-bromoaniline and using the methodology employed in the synthesis of dppm-d_{8ortho}, we successfully prepared the desired diphosphine in an overall yield of 42%. The synthetic details for dppm-d_{4ortho} are shown in eq 3, and the NMR and mass spectral data are in accord with the formulated structure.

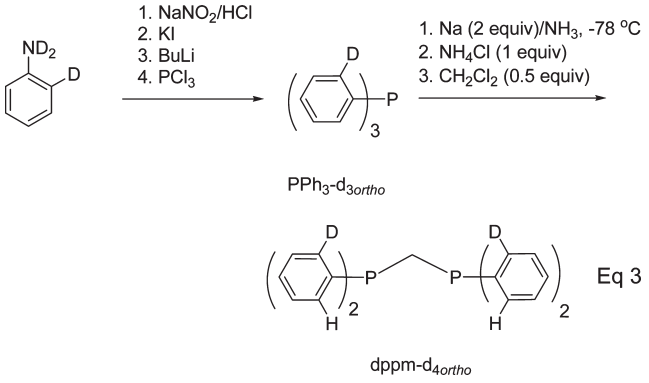

Eq 3

Treatment of $Os_3(CO)_{10}(MeCN)_2$ with dppm-d_{4ortho} furnished the diphosphine-substituted cluster $Os_3(CO)_{10}$(dppm-d_{4ortho}) in 72% yield after recrystallization. This cluster serves as a suitable platform for the investigation of the kinetic selectivity attendant in the ortho metalation, provided the unsaturated cluster $Os_3(CO)_9$(dppm-d_{4ortho}), the presumed precursor to the π/agostic complex, can be generated under mild conditions. While thermolysis of $Os_3(CO)_{10}$(dppm-d_{4ortho}) at temperatures in excess of 100 °C is expected to proceed with loss of CO and the formation of $Os_3(CO)_9$(dppm-d_{4ortho}), the harsh conditions will afford a thermodynamic mixture of the corresponding hydride and deuteride clusters $HOs_3(CO)_9[\mu$-(Ph-d_{1ortho})$P(C_6H_3D)CH_2PPh$-$d_{2ortho}]$ and $DOs_3(CO)_9[\mu$-(Ph-d_{1ortho})$P(C_6H_4)CH_2PPh$-$d_{2ortho}]$. No useful information concerning the kinetic aspects of the ortho metalation can be obtained under these conditions.

The photolysis of $Os_3(CO)_{10}$(dppm) was next explored as a potential route to $HOs_3(CO)_9[\mu$-$PhP(C_6H_4)CH_2PPh_2]$ before we conducted our experiments with the isotopically substituted cluster $Os_3(CO)_{10}$(dppm-d_{4ortho}). Near-UV photolysis of $Os_3(CO)_{10}$(dppm) in benzene-d_6 at room temperature in sealed NMR tubes produced liminal evidence for ortho metalation. Purging the liberated CO from solution with argon during photolysis facilitated the formation of the ortho-metalated product when the sample was irradiated for 24 h, but the yield was low (< 5%) and the time scale for the reaction was deemed impractical for our studies. The argon purge prevents the unsaturated $Os_3(CO)_9$(dppm) cluster from scavenging the released CO and regenerating $Os_3(CO)_{10}$(dppm). Accompanying the formation of the expected ortho-metalation product $HOs_3(CO)_9[\mu$-$PhP(C_6H_4)CH_2PPh_2]$ is the dimetalated cluster $HOs_3(CO)_8[\mu$-$PhP(C_6H_4$-$\mu_2,\eta^1)CH_2PPh_2]$, which presumably derives from the photochemically promoted loss of CO in the former cluster. This supposition was subsequently confirmed by a control experiment where $HOs_3(CO)_9[\mu$-$PhP(C_6H_4)CH_2PPh_2]$ was irradiated under similar conditions and found to give the octacarbonyl cluster. Although no quantum limits have been measured for these reactions, qualitatively $HOs_3(CO)_9[\mu$-$PhP(C_6H_4)CH_2PPh_2]$ appears to be more photosensitive than $Os_3(CO)_{10}$(dppm) with respect to CO loss. $Os_3(CO)_{10}$(dppm) is extremely photosensitive to 254 nm light (UV), and the cluster compounds $HOs_3(CO)_{8,9}[\mu$-$PhP(C_6H_4)CH_2PPh_2]$ were observed as the major products under controlled photolysis (i.e., short irradiation times and active CO purge).

One more experimental aspect had to be established before the ortho-metalation study using $Os_3(CO)_{10}$(dppm-d_{4ortho}) could be carried out. We had to be sure that the hydride and deuteride clusters $HOs_3(CO)_{8,9}[\mu$-(Ph-d_{1ortho})$P(C_6H_3D)CH_2$-PPh-$d_{2ortho}]$ and $DOs_3(CO)_{8,9}[\mu$-(Ph-d_{1ortho})$P(C_6H_4)CH_2$-PPh-$d_{2ortho}]$ could be accurately and easily quantified by ^{1}H NMR spectroscopy. In principle, NMR analysis using the hydrogens on the metalated aryl ring would permit a direct assessment of the isotopic composition associated with the ortho-metalation products $HOs_3(CO)_9[\mu$-(Ph-d_{1ortho})$P(C_6H_3D)$-CH_2PPh-$d_{2ortho}]$ and $DOs_3(CO)_9[\mu$-(Ph-d_{1ortho})$P(C_6H_4)CH_2$-PPh-$d_{2ortho}]$ and the corresponding octacarbonyl hydride/deuteride clusters. The formation of the latter clusters is not expected to involve any change in the isotope ratio from the nonacarbonyl hydride/deuteride clusters, as the conversion only involves a loss of CO. Unfortunately, the chemical shift data for the aryl hydrogens on the metalated ring have not been reported prior to this study. This problem was alleviated through a ^{1}H COSY analysis of $HOs_3(CO)_9[\mu$-$PhP(C_6H_4)CH_2PPh_2]$ and $HOs_3(CO)_8[\mu$-$PhP(C_6H_4)CH_2PPh_2]$ recorded in toluene-d_8, with the spectral assignments receiving additional corroboration by the NMR data in hand from the dppm-d_8 isotopomers of these clusters (*vide supra*). The structures shown below report the ^{1}H chemical shift data for the hydrogens on the aryl ring of interest. Both clusters exhibit an ABMX spin system for the hydrogens on the metalated ring, where the lowest field resonance may be confidently

(57) We have purified $DOs_3(CO)_8[\mu$-(Ph-d_{2ortho})$P(C_6H_3D$-$\mu_2,\eta^1)$-CH_2PPh_2-$d_{4ortho}]$ by recrystallization and column chromatography, albeit with some material loss using the former method. Both purification methods afforded indistinguishable NMR spectra. The ^{1}H NMR spectrum of the chromatographed cluster was critically scrutinized due to reports of isotope loss from facile H/D exchange between the stationary phase and the metal-deuteride species. See ref 58.

(58) (a) Keister, J. B.; Shapley, J. R. *J. Am. Chem. Soc.* **1976**, *98*, 1056. (b) Andrews, M. A.; Kirtley, S. W.; Kaesz, H. D. *Inorg. Chem.* **1977**, *16*, 1556.

(59) Here the k_{obsd} values of 5.33(1) and 4.98(2) $\times$ 10^{-4} s^{-1} were obtained by nonlinear regression analysis of the optical changes in the 600 and 386 nm band, respectively, from two different experiments. These data were averaged to give the quoted k_{obsd} value.

(60) (a) Parkin, G.; Bercaw, J. E. *Organometallics* **1989**, *8*, 1172. (b) Bullock, R. M.; Headford, C. E. L.; Hennessy, K. M.; Kegley, S. E.; Norton, J. R. *J. Am. Chem. Soc.* **1989**, *111*, 3897. (c) Janak, K. E.; Churchill, D. G.; Parkin, G. *Chem. Commun.* **2003**, 22. (d) Jones, W. D. *Acc. Chem. Res.* **2003**, *36*, 140.

(61) While a single elementary process involving the reductive coupling reaction cannot be definitively excluded, we consider this scenario unlikely given the totality of the available data. See refs 1, 2, 7, and 60.

(62) We acknowledge the possibility of a cluster intermediate having an agostic C−H(D) interaction with the aryl moiety as a viable preequilibrium species, but we can make no kinetic distinction between these two aryl-tethered species based on the data at hand.

(63) (a) Wolfsberg, M. *Acc. Chem. Res.* **1972**, *7*, 225. (b) Kubas, G. J. *Metal Dihydrogen and σ-Bond Complexes*; Kluwer Academic/Plenum Publishers: New York, 2001.

(64) For a few examples involving structurally and spectroscopically characterized π-bound metal compounds, see: (a) Jones, W. D.; Dong, L. *J. Am. Chem. Soc.* **1989**, *111*, 8722. (b) Cheng, T.-Y.; Szalda, D. J.; Bullock, R. M. *Chem. Chem.* **1999**, 1629. (c) Johansson, L.; Tilset, M.; Labinger, J. A.; Bercaw, J. E. *J. Am. Chem. Soc.* **2000**, *122*, 10846. (d) Norris, C. M.; Templeton, J. L. *Organometallics* **2004**, *23*, 3101.

(65) For an example of bimetallic cooperativity in an ortho-metalation process that exhibits an inverse isotope effect, see: Esswein, A. J.; Veige, A. S.; Piccoli, P. M. B.; Schultz, A. J.; Nocera, D. G. *Organometallics* **2008**, *27*, 1073.

assigned to H_a. With the exception of H_c in $HOs_3(CO)_8[\mu$-$PhP(C_6H_4)CH_2PPh_2]$, whose resonance is obscured by other aryl hydrogens, all of the metalated hydrogens appear as distinct resonances, and this allows these hydrogens to be used as internal markers in the determination of the ortho-metalation products generated during photolysis.

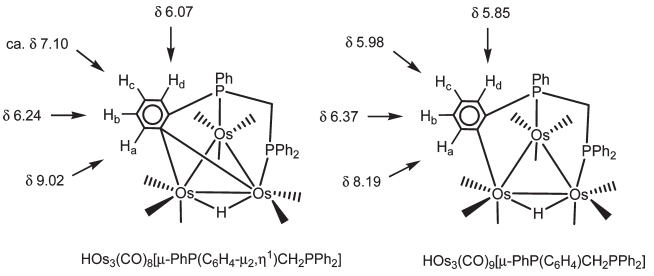

Photolysis of $Os_3(CO)_{10}$(dppm-d_{4ortho}) at 254 nm in toluene-d_8 at 275 K gave $HOs_3(CO)_9[\mu$-(Ph-d_{1ortho})P-$(C_6H_3D)CH_2PPh$-$d_{2ortho}]$ and $DOs_3(CO)_9[\mu$-(Ph-d_{1ortho})P-$(C_6H_4)CH_2PPh$-$d_{2ortho}]$ in 8.8% combined yield and HOs_3-$(CO)_8[\mu$-(Ph-d_{1ortho})P$(C_6H_3D$-$\mu_2,\eta^1)CH_2PPh$-$d_{2ortho}]$ and $DOs_3(CO)_8[\mu$-(Ph-d_{1ortho})P$(C_6H_4$-$\mu_2,\eta^1)CH_2PPh$-$d_{2ortho}]$ in 12% combined yield after 1 h.[66,67] The hydride:deuteride isomer ratio for both sets of products was found to be 67:33 in favor of the hydride cluster. This ratio is identical to that value determined earlier by us in the thermally equilibrated ortho-metalated clusters obtained from $Os_3(CO)_{10}$(bpcd-d_{4ortho}).[14] Continued irradiation for an additional 1 h furnished the above products in ca. 15% and 38% yield, respectively, with an isomeric ratio of 70:30. No significant change in the hydride:deuteride ratio in the cluster products was observed when the sample was next briefly heated at 323 K. The only noticeable reaction involved the conversion of some of the nonacarbonyl to the octacarbonyl cluster. After heating, the NMR tube was charged with CO and allowed to sit overnight at room temperature in the dark. NMR analysis the following day revealed the presence of only unreacted $Os_3(CO)_{10}$-(dppm-d_{4ortho}) and $HOs_3(CO)_9[\mu$-(Ph-d_{1ortho})P$(C_6H_3D)CH_2$-PPh-$d_{2ortho}]$ and $DOs_3(CO)_9[\mu$-(Ph-d_{1ortho})P$(C_6H_4)CH_2PPh$-$d_{2ortho}]$, as the octacarbonyl products were completely consumed. The hydride:deuteride isotope ratio for the nonacarbonyl clusters was determined to be 72:28. We also investigated the photolysis reaction at 243 K with the hopes of kinetically stabilizing the initially formed ortho-metalation products. Irradiation of $Os_3(CO)_{10}$(dppm-d_{4ortho}) for 3 h, followed by NMR analysis at the same temperature, revealed the presence of $HOs_3(CO)_8[\mu$-(Ph-d_{1ortho})P$(C_6H_3D$-$\mu_2,\eta^1)$-CH_2PPh-$d_{2ortho}]$ and $DOs_3(CO)_8[\mu$-(Ph-d_{1ortho})P$(C_6H_4$-$\mu_2,\eta^1)CH_2PPh$-$d_{2ortho}]$ in ca. 5% yield and an isotopic ratio of 70:30 for the hydride:deuteride clusters. The absence of nonacarbonyl products is attributed to the greater photochemical sensitivity of the nonacarbonyl clusters, which in turn lose CO rapidly to afford the observed octacarbonyl clusters. Finally, we also explored the photolysis at 201 K (dry ice/EtOH), but no ortho metalation was observed when the sample was irradiated for an extended period of time. The absence of ortho metalation at the lowest temperature may reflect an enhanced geminate recombination of the released CO and $Os_3(CO)_9$(dppm-d_{4ortho}).[68]

The ineludible conclusion that must be drawn from the above NMR experiments is the fact that the ortho-metalation products have undergone thermal equilibration during the time scale of these reactions. The initially formed products from C−H(D) bond activation are not stable and must undergo a rapid and reversible equilibration via a labile cluster intermediate(s). Scheme 5 outlines the gross aspects of a scenario that agree with the photolysis experiments. Optical excitation of $Os_3(CO)_{10}$(dppm-d_{4ortho}) leads to loss of CO and formation of the unsaturated cluster $Os_3(CO)_9$-(dppm-d_{4ortho}), followed by ortho metalation. Since the ortho metalation mandates the capping of one of the triangular Os_3 faces by the diphosphine ligand, the ancillary diphosphine in the $Os_3(CO)_{10}$(dppm-d_{4ortho}), which is equatorially disposed, must undergo a conformational change prior to ortho metalation, a feature that is addressed by the DFT calculations presented in the next section.

V. Calculation of the Mechanism for Ortho Metalation. We now turn our attention to the reaction of $HOs_3(CO)_9[\mu$-$PhP(C_6H_4)CH_2PPh_2]$ (species **B1**) with CO to give Os_3-$(CO)_{10}$(dppm) (species **C1**). The conversion of **B1** to **C1** is complex and occurs in three discrete stages: (1) reductive coupling, (2) ligand rearrangement, and (3) CO capture. The order of these steps is critical, and the fine points of each portion of the reaction warrant a thorough discussion. The labeling scheme for **B1** shown below will serve to aid the forthcoming DFT discussions.

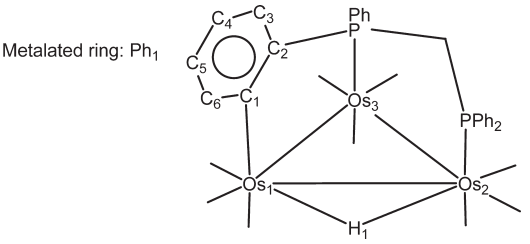

That **B1** functions as the nomological platform for C−H reductive coupling, and formation of species **B2** was quickly established through an appropriate step-scan analysis. The transition state **TSB1B2** differs from **B1** considerably, with the Os_2-H_1 bond distance increasing from 1.80 to 2.27 Å and the Os_1-H_1 distance decreasing from 1.87 to 1.82 Å as the C_1-H_1 bond forms, whose distance of 1.39 Å indicates that this bond has not completely formed. A counterclockwise tilting of the Ph_1 ring relative to the metallic plane facilitates the reductive coupling and allows the incipient agostic bond to adopt a favorable orientation relative to the Os_1 center.[69] Figure 5 shows the free-energy profile for this

(66) This experiment was also conducted with 1,4-di-*tert*-butylbenzene as an internal standard, and no significant material loss was noted. The uncertainty in the reported percent yields and the hydride:deuteride ratios is conservatively estimated as ±5%.

(67) Integration of the upfield hydride resonance belonging to the clusters $HOs_3(CO)_{8,9}[\mu$-(Ph-d_{1ortho})P$(C_6H_3D)CH_2PPh$-$d_{2ortho}]$ relative to any of the hydrogens on the metalated aryl ring also provides an independent check of the hydride:deuteride ratios in these two clusters. Accurate integration information is obtained only after waiting the customary delay period of five T_1 between acquisitions. The T_1 values for the different hydrogens were determined by performing a standard inversion−recovery experiment on $HOs_3(CO)_9[\mu$-$PhP(C_6H_4)CH_2PPh_2]$ and $HOs_3(CO)_8[\mu$-$PhP(C_6H_4$-$\mu_2,\eta^1)CH_2PPh_2]$ in toluene-d_8. The T_1 value measured from the bridging hydride group in these clusters is ca. 1.5 s and ca. 4.7 s, respectively.

(68) For a report on the temperature-dependent photochemistry in a tetraruthenium cluster, see: Yamamoto, S.; Asakura, K.; Mochida, K.; Nitta, A.; Kuroda, H. *J. Phys. Chem.* **1993**, *97*, 565.

(69) Here the tilt angle is defined by the atoms $Os_1-C_1-C_4$ and decreases from 176° (**B1**) to 161° (**TSB1B2**).

Scheme 5

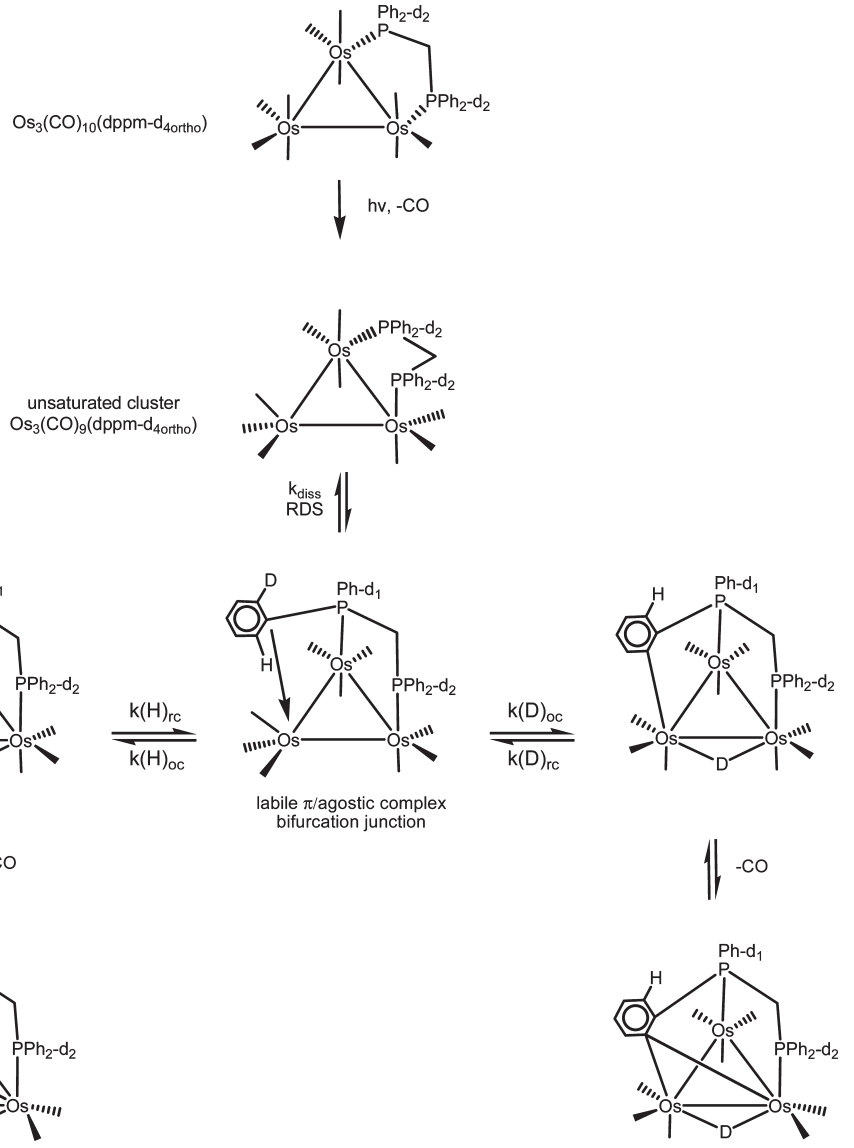

and the subsequent steps leading to **C1**, with Figure 6 showing the DFT-optimized geometric structures. An IRC calculation performed on **TSB1B2** confirmed that **B1** leads to the agostic compound **B2**, whose Os_1-H_1 distance of 2.093 Å and an $Os_1-H_1-C_1$ bond angle of 109.0° are in good agreement with the published criteria for an agostic M−C−H linkage.[70] While agostically bound substrates at mononuclear compounds are well established, their observation in metal clusters is rare. Deeming and Kabir have presented compelling NMR data for the participation of the agostic silane species $Os_3(HSiR_3)(CO)_9(dppm)$ in the reversible isomerization of $HOs_3(SiR_3)(CO)_9(dppm)$.[10e] **B2** resembles **TSB1B2** with further tilting of the Ph_1 ring to 142° and an elongation of the Os_1-C_1 bond to 2.67 Å. The C_1-H_1 bond distance of 1.12 Å is only slightly longer than the C−H bond distance of 1.084(6) Å found in benzene.[71] Continued tilting of the Ph_1 ring in **B2** to 104° furnishes an aryl group that is nearly orthogonal to the metallic plane and leads to the first of two distinct η^2-π complexes, **B3** and **B4**. The main difference between **B3** and **B4** involves the turnstile-type rotation of the aryl moiety and the three CO groups at Os_1 that leads to the exposure of the Os_1 center opposite the dppm ligand in the latter isomer. All species from **B1** through **B4** and their transition states are coordinatively saturated and contain 48*e*.

The second stage in the mechanistic pathway involves the rearrangement of the dppm ligand and proceeds from **B4** to **B5** via **TSB4B5**. This transition state represents the highest barrier in the overall process en route to **C1**. **TSB4B5** lies 21.6 kcal/mol above **B1** in energy, and its computed value is in good agreement with the $\Delta G^{\ddagger}_{298}$ value of 25 kcal/mol extrapolated from the experiments involving the carbonylation of $HOs_3(CO)_9[\mu\text{-}PhP(C_6H_4)CH_2PPh_2]$ to $Os_3(CO)_{10}(dppm)$ (*vide supra*). The transformation from **B4** to **TSB4B5** is accompanied by significant ligand redistribution about the cluster polyhedron. Here, an in-plane migration of two CO groups about the Os_1-Os_3 vector, coupled with the release of the π-bound arene moiety and an axial to equatorial permutation of the phosphine ligand at Os_3, is reflected in the

(70) (a) Brookhart, M.; Green, M. L.; Parkin, G. *Proc. Natl. Acad. Sci. U.S.A.* **2007**, *104*, 6908. (b) Lein, M. *Coord. Chem. Rev.* **2009**, *253*, 625.

(71) *Handbook of Chemistry and Physics*, 56th ed.; Weast, R. C., Ed.; CRC Press: Cleveland, OH, 1975.

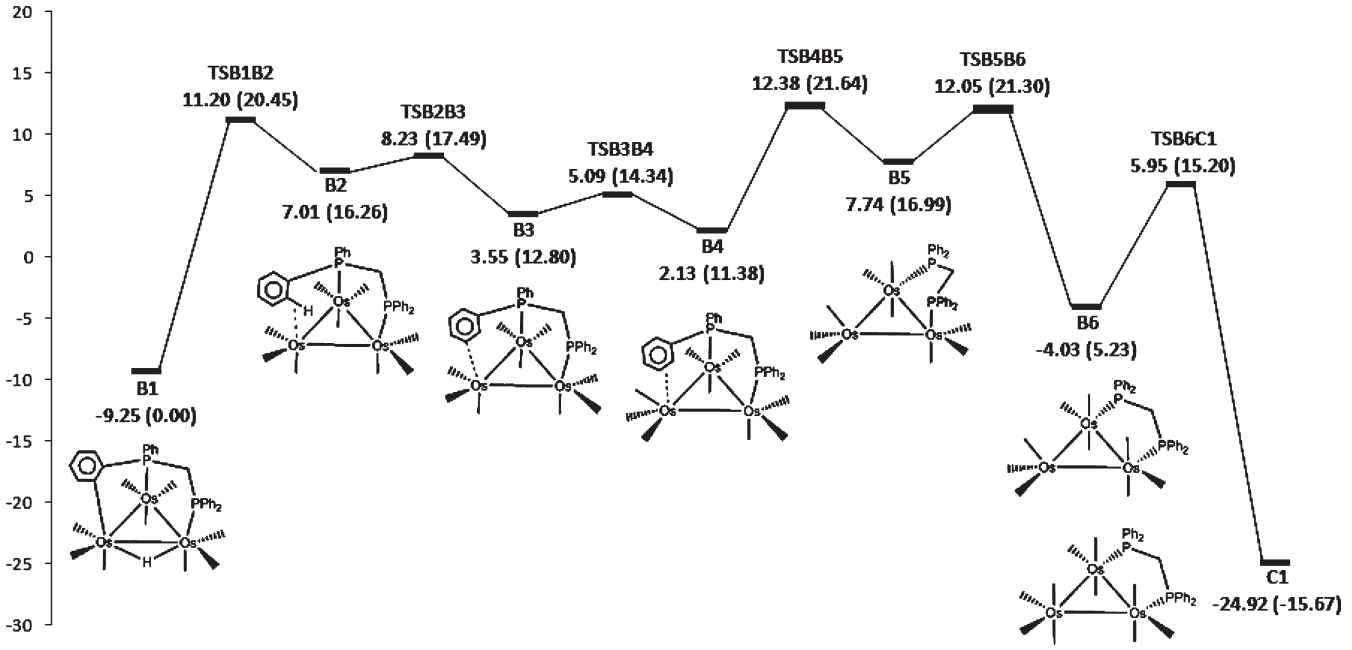

Figure 5. Potential energy surface for conversion of **B1** to **C1** in the presence of CO. Energy values are ΔG's in kcal/mol with respect to **A1** (**B1**).

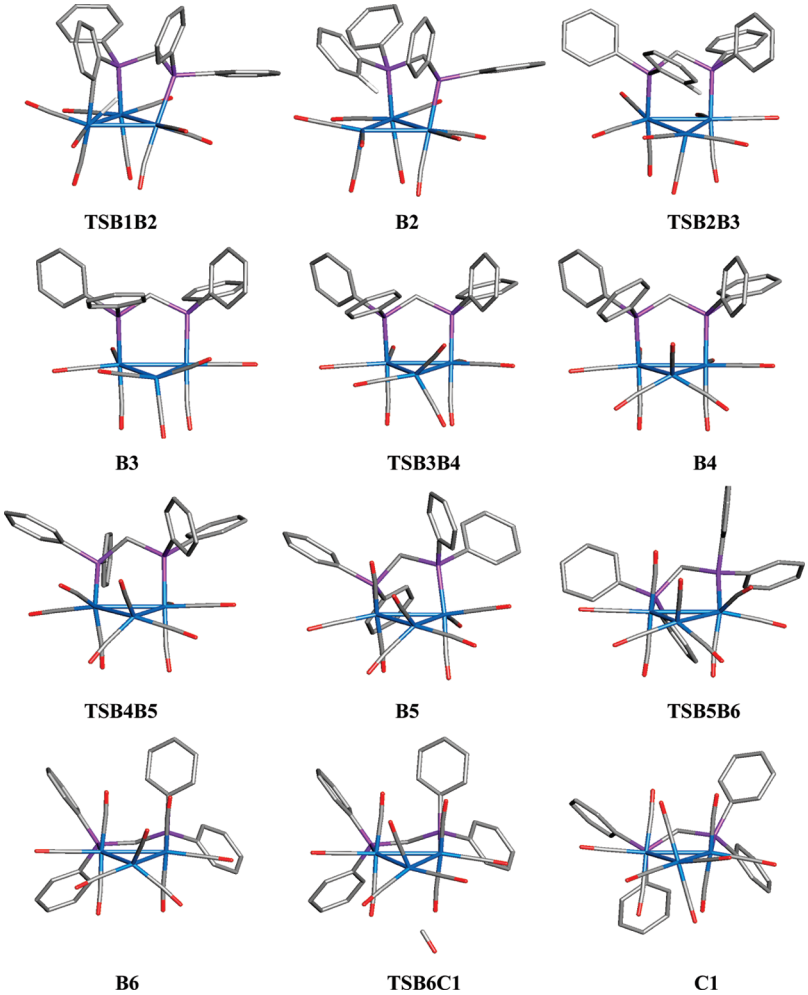

Figure 6. Optimized B3LYP structures for the intermediates **B2**−**B6** and **C1** and the corresponding transition states.

optimized structure of **TSB4B5**. The pairwise exchange of CO groups about the Os_1-Os_3 vector is not unexpected and, in fact, has a phenomenological foundation that is documented by ^{13}C NMR studies on the fluxional behavior of

CO ligands in numerous polynuclear clusters.[72] $Os_3(CO)_9$-(dppm-P_a,P_e) (**B5**) is coordinatively unsaturated by virtue of its 46*e* count, and its reaction with CO will be considered shortly in detail. The remaining axial phosphine moiety at Os_2 relaxes to an equatorial disposition by an analogous CO exchange process about the Os_1-Os_2 vector to afford Os_3-$(CO)_9$(dppm-P_e,P_e) (**B6**), which lies 5.2 kcal/mol above **B1** in energy. The orientation of the three CO groups at Os_1 in **B6** is similar to that found in species **B4** and **B5**.

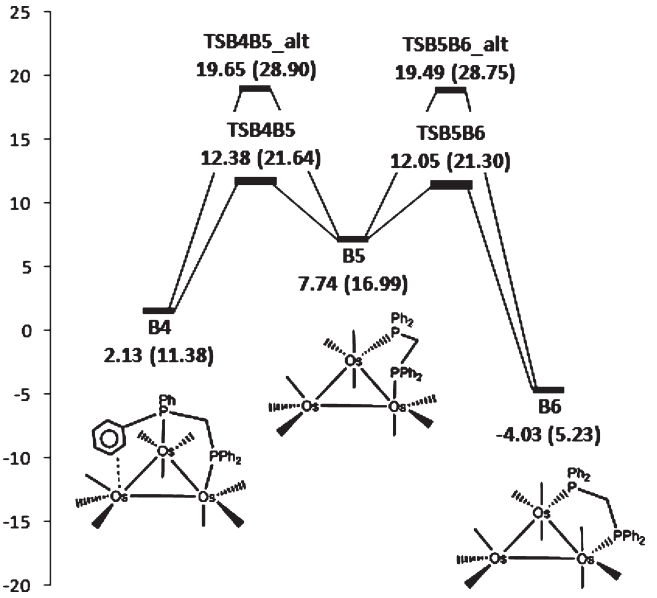

Figure 7. Potential energy surface for conversion of **B4** to **B6** depicting the lower energy in-plane migration and alternative tripodal rotation exchange schemes. Energy values are ΔG's in kcal/mol with respect to **A1** (**B1**).

The formation of **B5** from **B4** may also be envisioned through a process involving the localized scrambling of three of the four ligands at Os_3, and this possibility was investigated accordingly.[73] A tripodal exchange involving the axial phosphine and the two equatorial CO groups furnishes **B5** via the transition state **TSB4B5_alt**, as shown in Figure 7. Concurrent with the 3-fold scrambling of ligands at Os_3 is the release of the π-bound aryl ring that must accompany the phosphine moiety in its transit to the equatorial site orthogonal to the Os_3-Os_2 vector in **B5**. A similar exchange of phosphine and CO ligands at Os_2 completes the reaction sequence and gives **B6**. The computed energies of **TSB4B5_alt** and **TSB5B6_alt** are nearly identical, but more importantly they are considerably higher in energy in comparison with their in-plane migration counterparts already discussed. These computational data agree with the available VT NMR data on $Os_3(CO)_{12-n}P_n$ clusters where the tripodal exchange of phosphine and CO ligands reveals a higher free energy of activation compared with the in-plane migration sequence for ligand permutation.[72b,73]

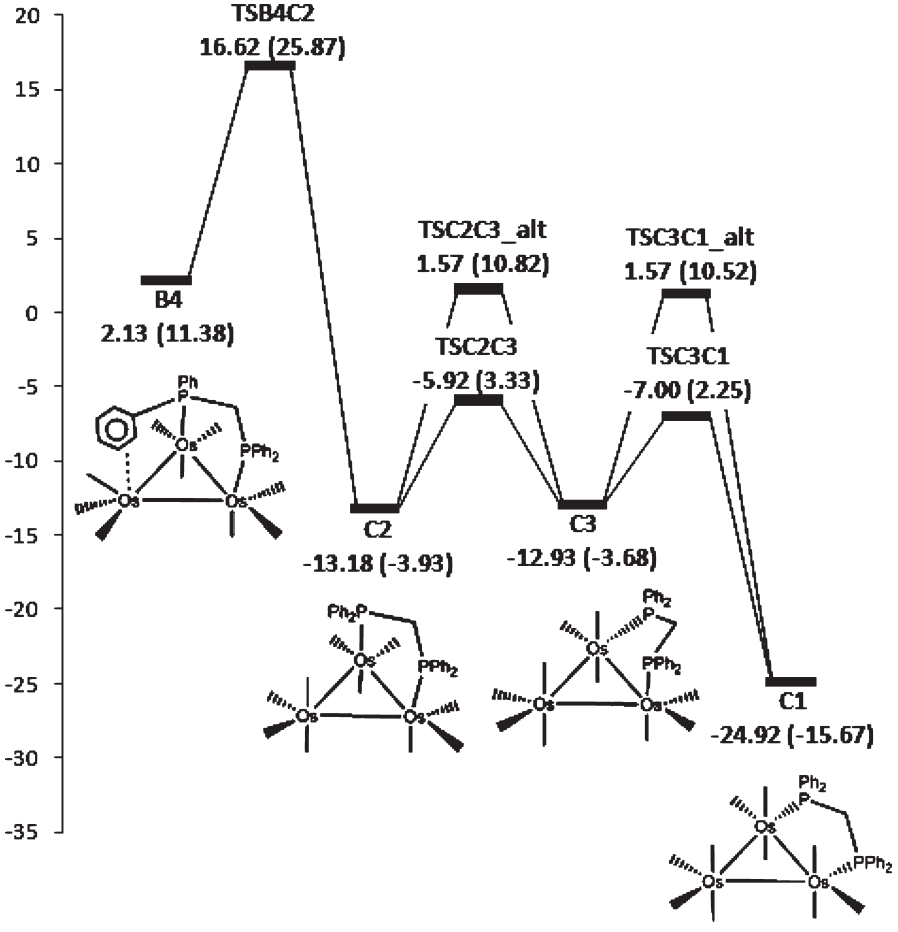

Figure 8. Potential energy surface for the alternative pathway involving the attack of CO on **B4** to give **C1**, including the lower energy in-plane migration and alternative tripodal rotation isomerization sequences. Energy values are ΔG's in kcal/mol with respect to **A1** (**B1**).

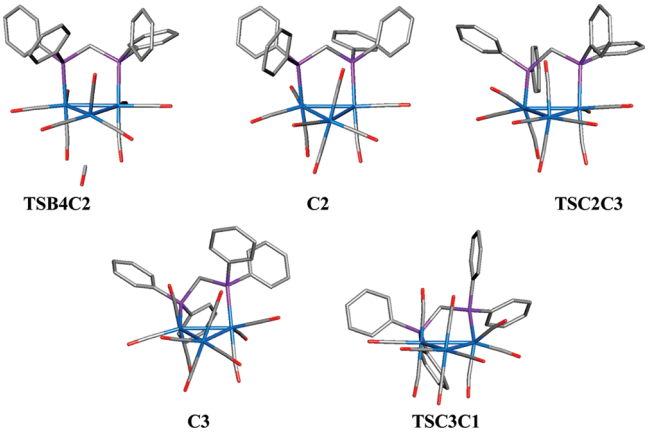

Figure 9. Fully optimized B3LYP structures for intermediates **C2** and **C3** and the corresponding transition states along the alternative pathway from **B4** to **C1**.

The scavenging of CO by **B6** completes the carbonylation reaction and affords the known cluster $Os_3(CO)_{10}$(dppm-P_e,P_e) (**C1**). The transition state associated with this substitution, **TSB6C1**, occurs early and is endergonic by ca. 10 kcal/mol relative to **B6**. The optimized structure computed for **C1** shows an excellent correspondence with the solid-state structure for $Os_3(CO)_{10}$(dppm).[74] As mentioned earlier, the rate-limiting step for the conversion of **B1** to **C1** is **TSB4B5**, with an overall $\Delta G^{\ddagger}$ = 21.64 kcal/mol. The mechanistic pathway reveals a first-order dependence on **B1** and is independent of CO, features in accord with the experimental data. Moreover, isotopic substitution of H_1 with deuterium gave a $\Delta\Delta G^{\ddagger}$ of 0.71 kcal/mol and an inverse isotope effect of 0.30 consistent with the experimentally measured isotope effect of 0.50.[75] The nature of the species in the preequilibrium, which was initially assumed to involve only a single π intermediate, may now be thoroughly addressed. The equilibria between species **B1**−**B4** give rise to the observed and computed EIE, and the events depicted in Figure 5 nicely account for the thermodynamic hydride/deuterium equilibration found in the photolysis of $Os_3(CO)_{10}$(dppm-d_{4ortho}). The transformation of **B4** to **B5** shows no significant isotope effect ($\Delta\Delta G^{\ddagger}$ = 0.01 kcal/mol), as expected for a process that does not involve the breaking of any isotopically sensitive bonds.

In this final section we address the reaction of CO with **B4** and probe the dynamics for the CO-promoted displacement of the π-bound aryl moiety from the Os_1 center. CO addition to the Os_1 center in **B4** affords the transition state **TSB4C2** and resembles those transition states computed for the addition of CO to **A2** and **B6**. This scenario is akin to an associative pathway where the rate-limiting step involves the attack of CO on **B4**.[76] The Os_1−π interaction has decreased slightly on the basis of the Os_1−C_2 and Os_1−C_3 bond distances of 3.97 and 4.20 Å, respectively, and **TSB4C2** lies 25.9 kcal/mol above **B1** in energy. Figures 8 and 9 illustrate these data. The dppm ligand exhibits axial coordination in **C2**, and this addition product is an isomer of **C1**. Tandem in-plane migrations of axial CO groups across the Os_1−Os_2 and Os_1−Os_3 vectors afford **C3** and **C1**, respectively, and this process serves as the lowest energy manifold for the stereochemical permutation of the two Ph_2P moieties. The alternative process involving sequential tripodal rotations proceeds through the higher energy transition states **TSC2C3_alt** and **TSC3C1_alt** and mimics those trends found in the conversion of **B4** → **B5** → **B6**. Energetically, the computed $\Delta G^{\ddagger}$ value of 25.9 kcal/mol (**TSB4C2**) is close to that computed for the dissociative manifold involving **B4** → **TSB4B5** ($\Delta G^{\ddagger}$ = 21.6), making a mechanistic distinction problematic in the absence of kinetic data.[77] Fortunately, the carbonylation kinetics confirmed the zero-order dependence of CO on the reaction, which allows us to eliminate the associative process from consideration.

Conclusions

The carbonylation kinetics for $HOs_3(CO)_8[\mu$-$PhP(C_6H_4$-$\mu_2,\eta^1)CH_2PPh_2]$ to $HOs_3(CO)_9[\mu$-$PhP(C_6H_4)CH_2PPh_2]$ have been investigated, and the reaction was found to be first-order in cluster and CO and does not exhibit any noticeable isotope effect. Of the two kinetically indistinguishable processes supported by the carbonylation data, DFT calculations have proven invaluable in terms of unraveling the kinetic enigma. It is shown that the dimetalated aryl moiety in $HOs_3(CO)_8[\mu$-$PhP(C_6H_4$-$\mu_2,\eta^1)CH_2PPh_2]$ is in equilibrium with the isomeric cluster $HOs_3(CO)_8[\mu$-PhP-$(C_6H_4$-$\eta^1)CH_2PPh_2]$, and it is the latter species that is attacked by CO. The carbonylation of $HOs_3(CO)_9[\mu$-$PhP(C_6H_4)CH_2$-$PPh_2]$ to $Os_3(CO)_{10}$(dppm) is independent of CO and displays an equilibrium isotope effect of 0.50. These data support a reductive coupling scenario involving, at a minimum, a preequilibrium species that precedes the rate-limiting formation of $Os_3(CO)_9$(dppm). DFT calculations indicate that C−H bond formation gives rise to an agostic intermediate, followed by two discrete π-aryl cluster species before the generation of the isomeric clusters $Os_3(CO)_9$-(dppm). The energy barrier between the different agostic and π intermediates is low (< 5 kcal/mol), and this accounts for the kinetic lability displayed by these species. The agreement between the experimental and computational data is impressive, and the utility of DFT calculations to provide unprecedented insight into complex bond-forming and bond-breaking reactions occurring at polynuclear metal clusters cannot be overemphasized.

Acknowledgment. Financial support from the Robert A. Welch Foundation (Grants A-0648-MBH and B-1093-MGR) and the National Science Foundation (CHE-0518074, CHE-0541587, and DMS-0216275) is greatly appreciated. Profs. Shariff E. Kabir and Manfred Schlosser

(72) (a) Adams, R. D.; Cotton, F. A. In *Dynamic Nuclear Magnetic Resonance Spectroscopy*; Jackman, L. M., Cotton, F. A., Eds.; Academic Press: New York, 1975; Chapter 12. (b) Alex, R. F.; Pomeroy, R. K. *Organometallics* **1987**, *6*, 2437. (c) Cooke, J.; Takats, J. *Organometallics* **1995**, *14*, 698.

(73) This process has also been referred to as a restricted trigonal twist and has been observed in different $Os_3(CO)_{12-n}P_n$ clusters (where n = 1−4) containing monodentate phosphine/phosphite ligands. See: (a) Deeming, A. J.; Donovan-Mtunzi, S.; Kabir, S. E. *J. Organomet. Chem.* **1985**, *281*, C43. (b) Ref 72b.

(74) Azam, K. A.; Hursthouse, M. B.; Kabir, S. E.; Abdul Malik, K. M.; Abdul Mottalib, M. *J. Chem. Crystallogr.* **1999**, *29*, 813.

(75) A rate-limiting step involving the conversion of **B1** to **B2** may be eliminated from consideration on the basis of the computed isotope effect. A normal KIE ($\Delta\Delta G^{\ddagger}$ = −0.60) has been computed for the single-step reductive coupling process, clearly incongruent with the isotope ratio experimentally determined for the carbonylation.

(76) Darensbourg, D. J. *Adv. Organomet. Chem.* **1982**, *21*, 113.

(77) The isotope effect for the associative process has been computed as 0.29, and this reflects the preequilibria involving species **B1**−**B4**. A mechanistic distinction based solely on this criterion is not possible.

are thanked for providing an initial sample of $HOs_3(CO)_8[\mu\text{-}PhP(C_6H_4\text{-}\mu_2,\eta^1)CH_2PPh_2]$ and helpful comments concerning the functional-group-directed deuteration of halo arenes, respectively. We also acknowledge the reviewers for helpful comments. Ms. Nicole Ledbetter (UNT) and Dr. Yongxuan Su (UCSD) are thanked for their assistance in recording the reported mass spectra of our isotopically substituted ligands and cluster compounds.

Supporting Information Available: Experimental details related to the synthesis of the deuterium-substituted intermediates employed in the preparation of the dppm-d_{8ortho} and dppm-d_{4ortho} ligands, spectroscopic data for selected clusters, plots of selected kinetic data, complete ref 25, 2-D scan for the **A1** to **B1** reaction surface, and atomic coordinates of all optimized stationary points and transition states. These materials are available free of charge via the Internet at http://pubs.acs.org.